**Forschungszentrum Karlsruhe**
Technik und Umwelt

**Wissenschaftliche Berichte**
FZKA 5710

# Assessment of Uncertainties in the Analysis of Molten Core-Concrete Interaction Using the WECHSL Code

**J. J. Foit, S. Schmidt-Stiefel**

**Institut für Angewandte Thermo- und Fluiddynamik**

**März 1997**

FORSCHUNGSZENTRUM KARLSRUHE
Technik und Umwelt
**Wissenschaftliche Berichte**
FZKA 5710

# Assessment of Uncertainties in the Analysis of Molten Core-Concrete Interaction Using the WECHSL Code

*J. J. Foit, S. Schmidt-Stiefel*
Institut für Angewandte Thermo- und Fluiddynamik

Forschungszentrum Karlsruhe GmbH, Karlsruhe
1997

Forschungszentrum Karlsruhe GmbH
Postfach 3640, 76021 Karlsruhe

ISSN 0947-8620

## Abstract

Accident sequences result in a broad variation of the initial conditions at the time of RPV failure. Additionally, there are uncertainties in the knowledge of the properties of corium melts, among others the viscosity, the solidus-liquidus temperatures, and the thermal conductivity of the ex-vessel oxide melts. Therefore, the initial conditions for the MCCI analysis are not very well known. The uncertainties consist in variations of

- the time of RPV failure;
- the initial melt temperature;
- the initial mass and melt compositions;
- the melt configuration (possibility of segregation of metal and oxide melts instead of homogeneous mixing);
- the rates of melt slumping from the RPV.

A PWR core melt accident scenario is used as the reference case to assess the uncertainties in WECHSL MCCI calculations which are caused by the variations mentioned above.

## Bewertung der Unsicherheiten in der Analyse der Kernschmelze-Beton-Wechselwirkung mit dem Rechenprogramm WECHSL


### Zusammenfassung

Verschiedene Unfallszenarien führen zu unterschiedlichen Anfangsbedingungen, die zum Zeitpunkt des RDB-Versagens herrschen werden. Eine zusätzliche Quelle von Unsicherheiten besteht in der unzureichenden Kenntnis von physikalischen Eigenschaften von Ex-vessel-Schmelzen, wie z. B. der Viskosität, der Solidus- und Liquidustemperatur und der Wärmeleitzahl. Aus diesen Gründen sind alle Annahmen, die für Analysen von schweren Reaktorunfällen gemacht werden, mit Unsicherheiten behaftet. Diese Unsicherheiten beziehen sich auf:

- den Zeitpunkt des RDB-Versagens;
- die Anfangstemperatur der Kernschmelze;
- die Anfangsmassen und deren Zusammensetzung;
- die Form der Schmelze (Metall und Oxid getrennt oder homogen vermischt);
- die Austrittsraten der Schmelze aus dem RDB.

Ein DWR-Unfallszenario diente als Ausgangsbasis, um die Auswirkungen der obengenannten Unsicherheiten auf die WECHSL-Ergebnisse zu untersuchen.

CONTENTS

## 1. Introduction

Two computer codes are available for modeling molten core-concrete interaction (MCCI). These codes may be considered as representing the state of the art. The CORCON code [1] originates from Sandia National Laboratories, U.S.A. The WECHSL code [2] was developed at KfK, Germany, a new version of which has recently been released. In addition to predicting concrete cavity erosion and the possibility of basemat penetration, the MCCI code output forms the basis of many calculations on containment and fission product release. Therefore, these codes play an important role in the assessment of the long-term effects of possible severe nuclear reactor accident scenarios.

In [3] plant application calculations of MCCIs were performed using the CORCON and WECHSL computer codes. The plant application of MCCI codes was investigated in a code comparison exercise. Three MCCI scenarios were chosen for this comparison exercise in order to study the consequences of the basemat erosion process as well as to identify the remaining uncertainties in the description of the short term and the long-term erosion processes.

The experimental programs SURC [4] at SNL (USA), ACE [5] at ANL (USA) and BETA II [6] at KfK (Germany) provided a database for further code validations [7], [8]. This assessment showed deficiencies in the knowledge of oxide melt properties, e. g. viscosity and solidus and liquidus temperatures as well as deficiencies in heat transfer modeling for oxide melts.

Therefore, the WECHSL modeling of oxide melts - concrete interactions was improved by including the effect of the melt temperature on the viscosity dependence of heat transfer together with a correlation which reduces the thermal conductivity of oxide melts to allow for the porosity of the debris [9]. In addition, the influence of Zr and Si on the solidus-liquidus temperatures of the metal melt was taken into account by simple inclusion of the Zr-Fe and Si-Fe phase diagrams in the ternary Fe-Cr-Ni phase diagram which was used in the WECHSL code. The former scheme used in WECHSL for advancing the cavity shape was improved in order to avoid an unphysical cavity shape which had been observed in some calculations. By this, the development of the WECHSL code is considered to be completed.

The accident sequences result in a broad variation of the initial conditions at the time of RPV failure. Additionally, there are uncertainties in the knowledge of the

properties of corium melts, among others the viscosity, the solidus-liquidus temperatures, and the thermal conductivity of the ex-vessel oxide melts. Therefore, the initial conditions for the MCCI analysis are not very well known [10].
The uncertainties consist in variations of

- the time of RPV failure;
- the initial melt temperature;
- the initial mass and melt compositions;
- the melt configuration (possibility of segregation of metal and oxide melts instead of homogeneous mixing);
- the rates of melt slumping from the RPV.

The purpose of this report is to study the influence of the uncertainties above on the results of the WECHSL calculations of MCCIs. In addition, some of the results of [3], which were obtained using the former WECHSL version, will be compared to the results of the improved WECHSL code used in the calculations presented here.

## 2. Low Pressure PWR Accident Scenario

The PWR plant, which was the subject of the investigations in the German Risk Study, Phase B [11], will also be used to assess the uncertainties in WECHSL MCCI calculations, which result from different initial conditions and different core melt properties used in the calculations.

### 2.1 Short Description of the Reference Scenario

In the low pressure accident sequence the core melt, which consists of oxides and metals, is expected to relocate into a cylindrical reactor cavity with an inner radius of 3.2m. In the scenario described here it is assumed that relocation takes place 7800 s after the reactor tripped. With this assumption, the heat generation in the oxide phase starts at 23.74 MW and in the metal phase at 3.24 MW. If the 0.9m thick self-supporting concrete cylinder fails, the molten pool will be flooded by sump water. The corium inventory at the start of the MCCI is shown in Table 1.

| Melt Constituent | Mass [kg] |
|---|---|
| Fe | $5.3 \times 10^4$ |
| Zr | $1.8 \times 10^4$ |
| Cr | $1.1 \times 10^4$ |
| Ni | $6.4 \times 10^3$ |
| $UO_2$ | $1.12 \times 10^5$ |
| $ZrO_2$ | $1.65 \times 10^4$ |

Table 1: Corium inventory

The initial melt temperature is estimated to be 2673 K. The reactor cavity and the 6 m thick basemat consist of siliceous type of concrete. Its properties are indicated in Table 2.

The decomposition temperature and the decomposition enthalpy are $T_{dec} = 1573$ K and $H_{dec} = 2.075 \times 10^6$ J/kg, respectively. The solidus-liquidus temperatures of the oxide phase were chosen to be the softening temperatures estimated in [12].

| Constituent | Weight Fraction |
|---|---|
| $SiO_2$ | 0.7655 |
| $Ca(OH)_2$ | 0.0728 |
| $CaCO_3$ | 0.0663 |
| $H_2O$ | 0.0422 |
| $Al_2O_3$ | 0.0532 |

Table 2: Composition of the silicious concrete

## 2.2 WECHSL Calculations

The analysis starts after the melt has penetrated the reactor pressure vessel and is contained in the dry reactor cavity. In the initial phase of melt/concrete interaction the dominant energy source in the melt is the energy released in the zirconium oxidation reaction with the concrete decomposition products. Two calculations were made for this scenario, one with a stratified melt configuration, i. e. an underlaying metal layer covered by an oxide layer, and one with a completely mixed melt.

### 2.2.1 Temperature, Crust Growth, and Heat Transfer

After an initial slow decrease, corresponding to the period of Zr oxidation, a rapid decline in the melt temperatures is predicted (Figures 1,2,3). After the initial rapid fall in the melt temperatures, the stratified melt calculation predicts an increase in the temperature of the oxide layer within about 17 hours followed by a slow decrease of the temperature whereas the mixed layer calculation predicts a temperature with a steady, very slow decline. For both melt configurations the WECHSL code predicts a plateau in the long term oxide melt temperature behavior at about 100 K above the liquidus temperature (Figures 4 and 5). This is in contrast to the finding in [3]. For the layered melt configuration, the interface temperature of the metal melt decreases to the solidus temperature during the first 900 s of the interaction and a metal bottom crust is formed. The increasing thickness of this crust considerably reduces the heat transfer from the metal to the concrete (Figure 6). The metal layer is predicted to be completely solidified within 32 hours (Figure 7). A top crust forms with the beginning of sump water ingression which is predicted to happen after 14.6 hours and 3 h for the layered and the mixed calculations, respectively (Figures 8 and 9). WECHSL does not predict a bottom crust for the mixed layer configuration. The distribution of the heat fluxes is given in Figure 10.

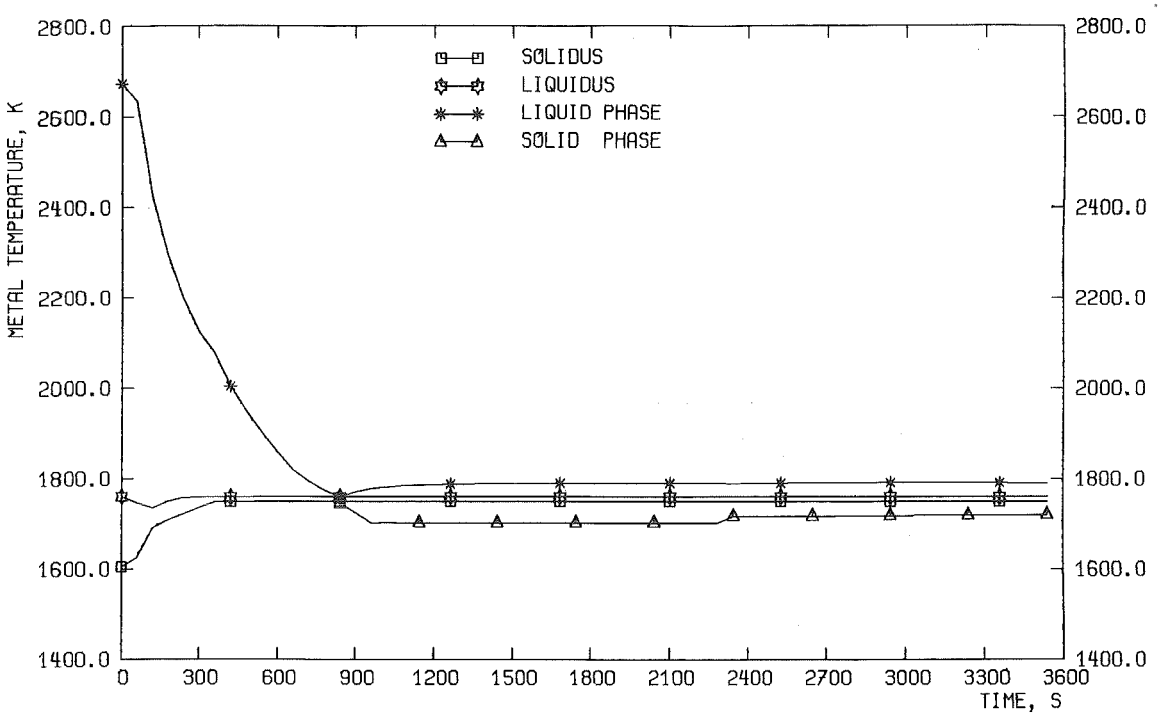


Fig. 1: PWR metal melt temperatures (layered calculation).

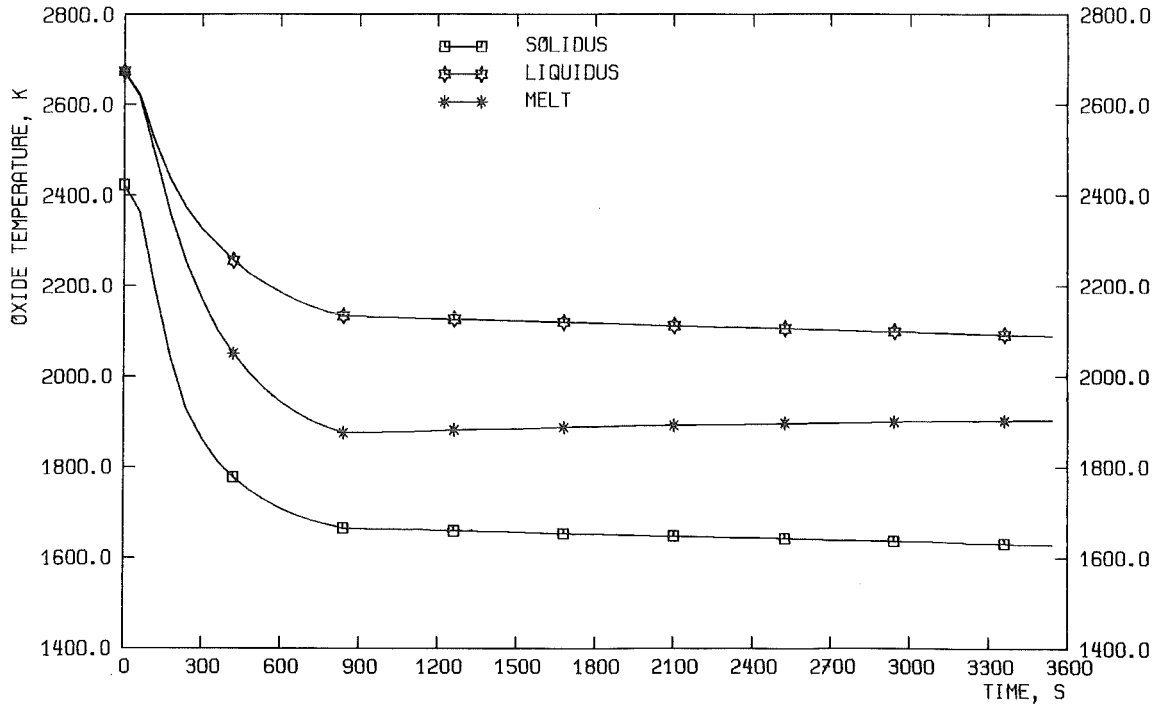


Fig. 2: PWR oxide melt temperatures (layered calculation).

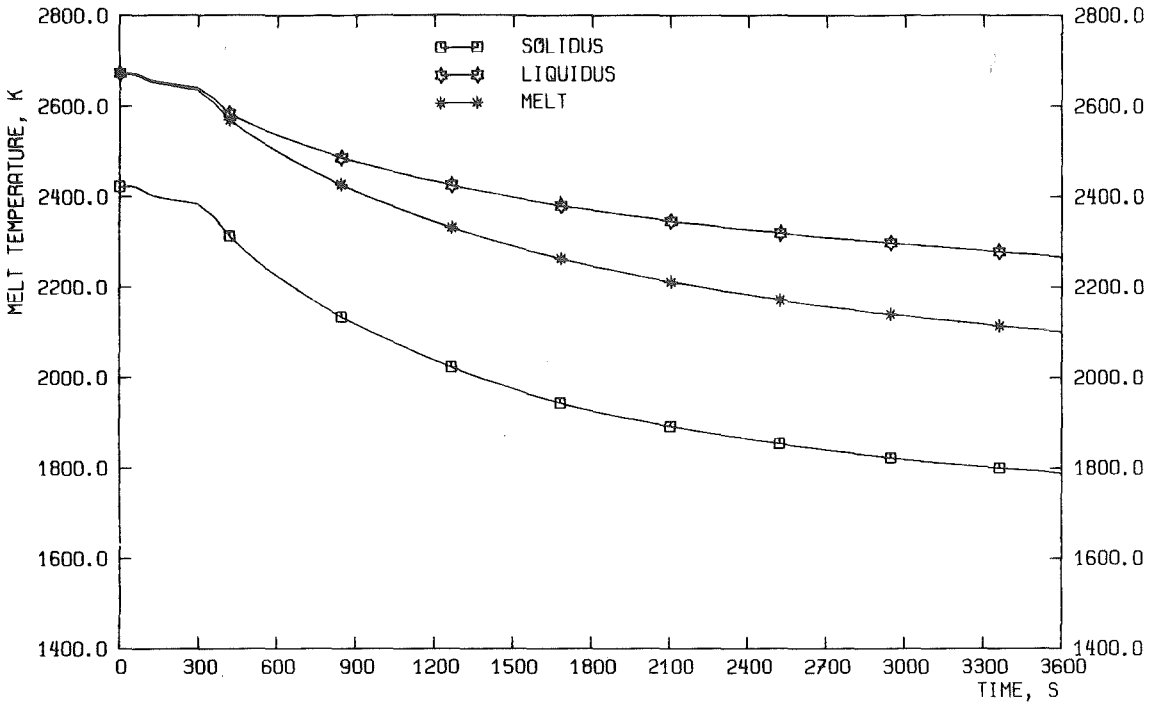


Fig. 3: PWR melt temperatures (mixed calculation).

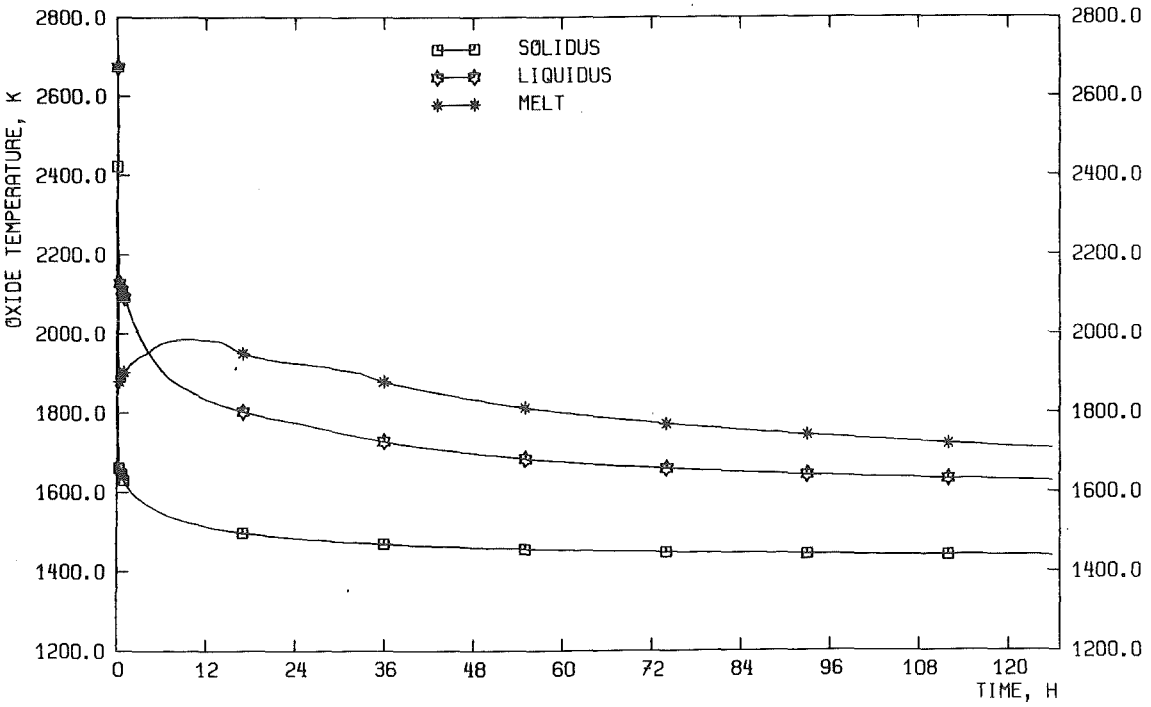


Fig. 4: PWR oxidic melt temperatures (layered calculation).

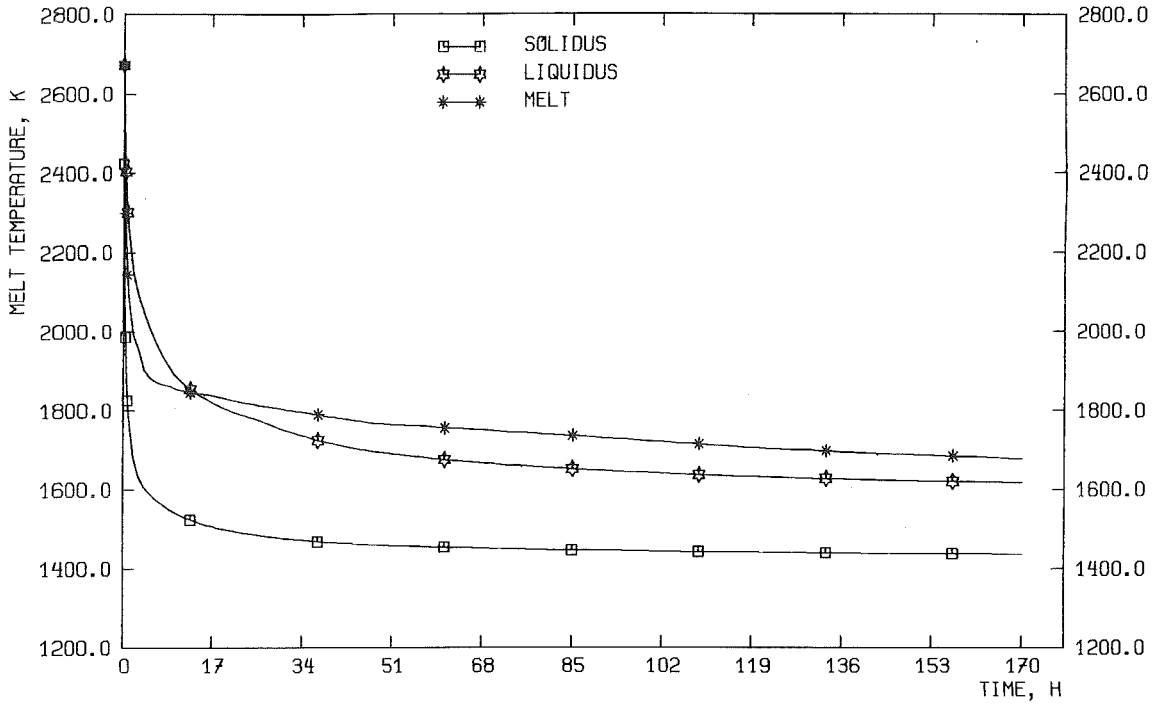


Fig. 5: PWR melt temperatures (mixed calculation).

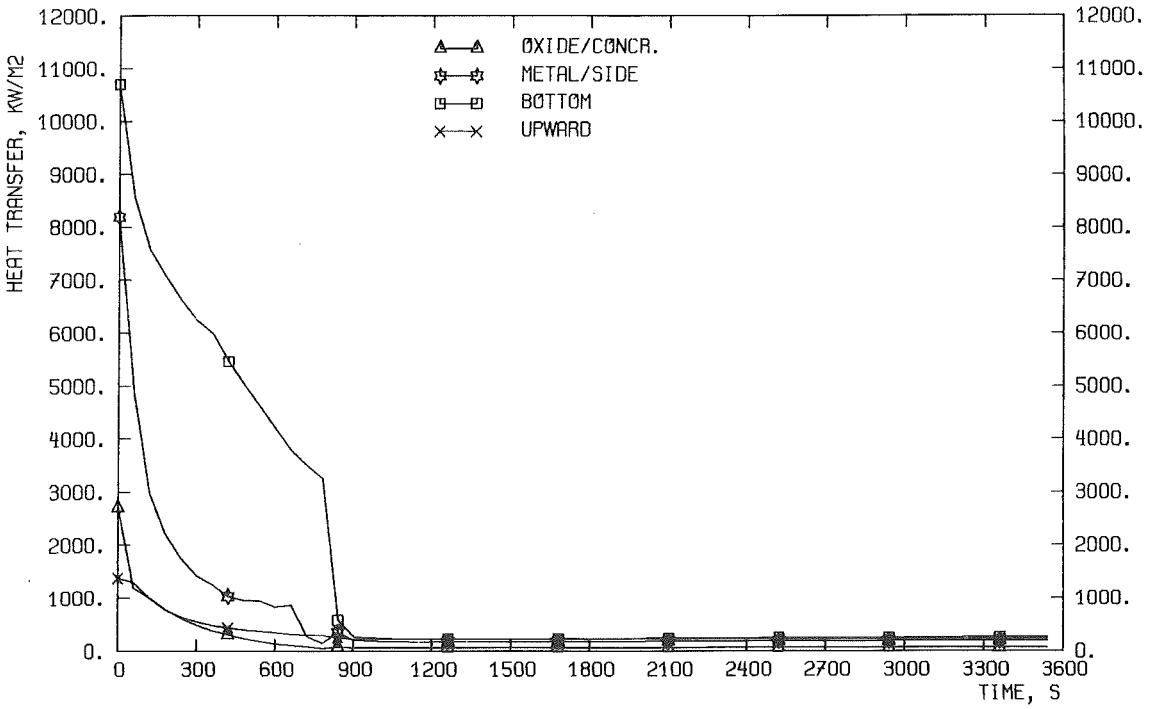


Fig. 6: PWR heat fluxes (layered calculation).

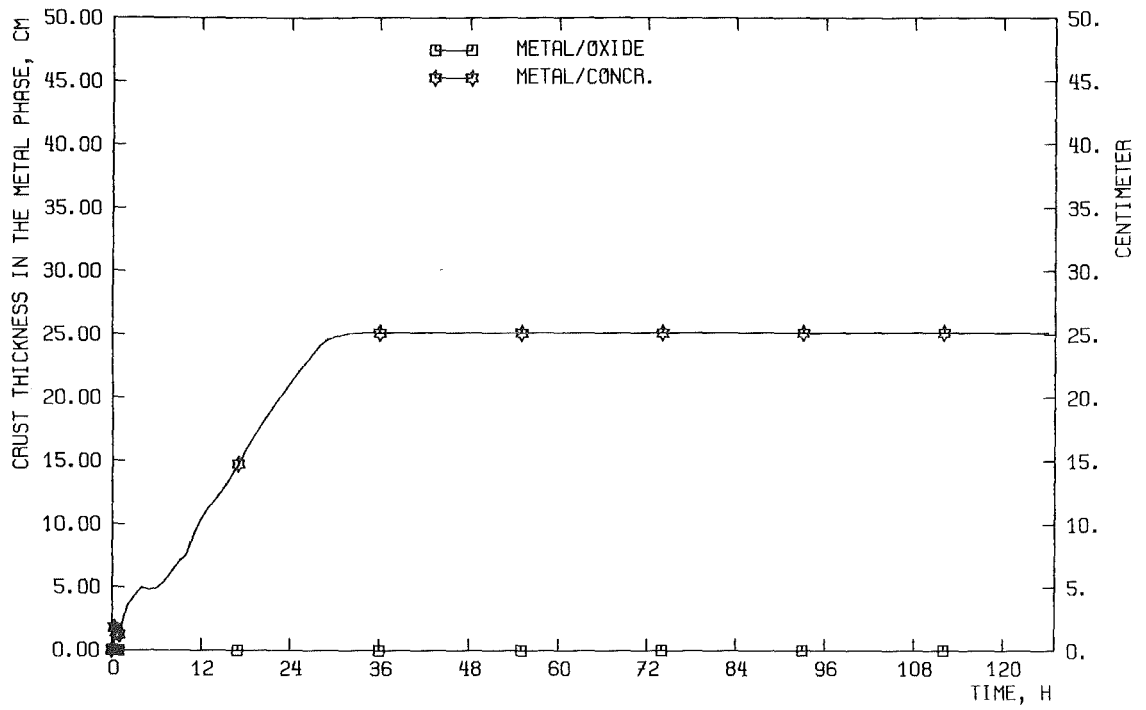


Fig. 7: PWR metal crusts (layered calculation).

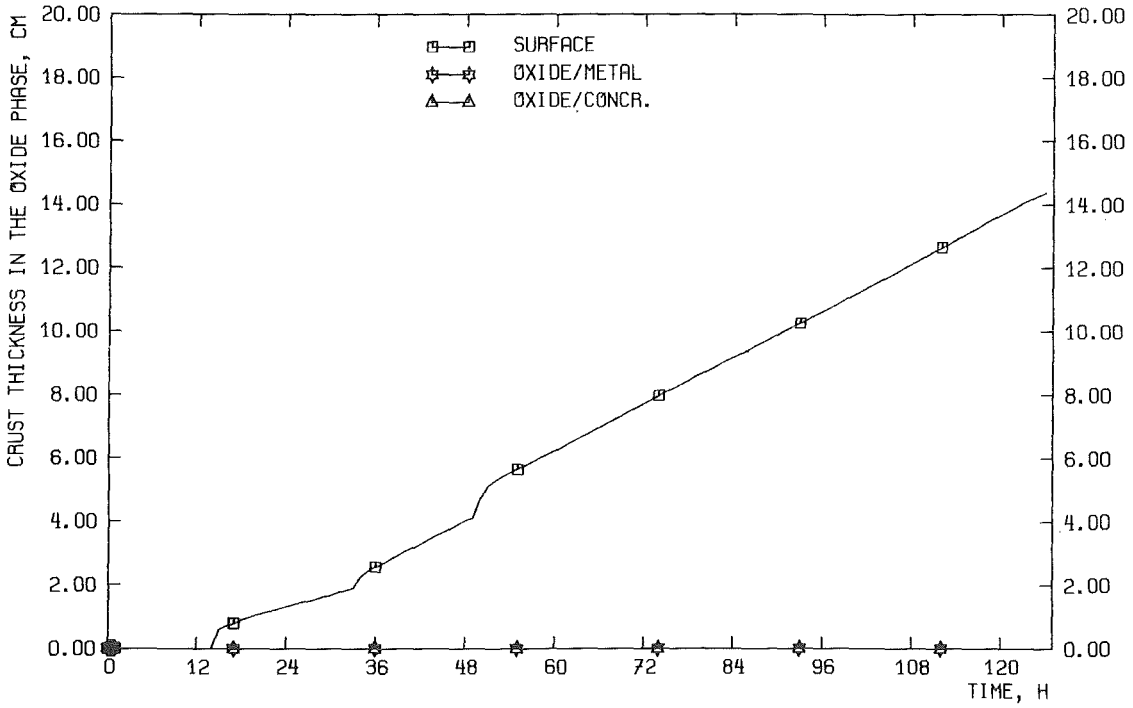


Fig. 8: PWR oxide crusts (layered calculation).

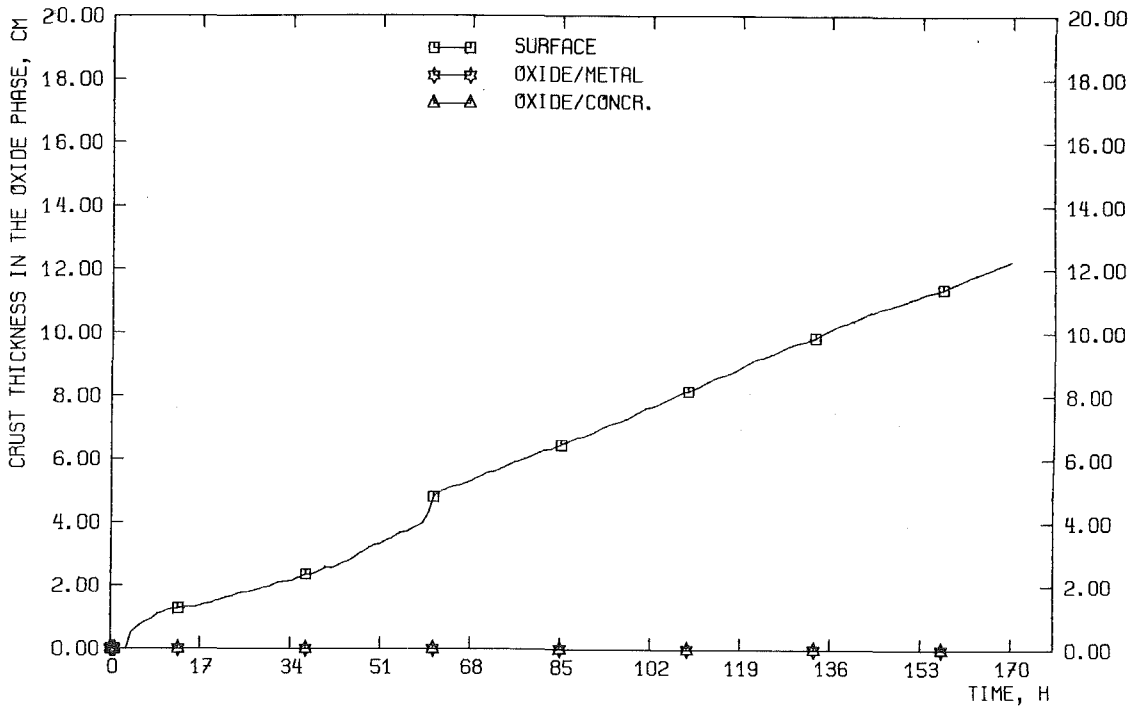


Fig. 9: PWR melt crusts (mixed calculation).

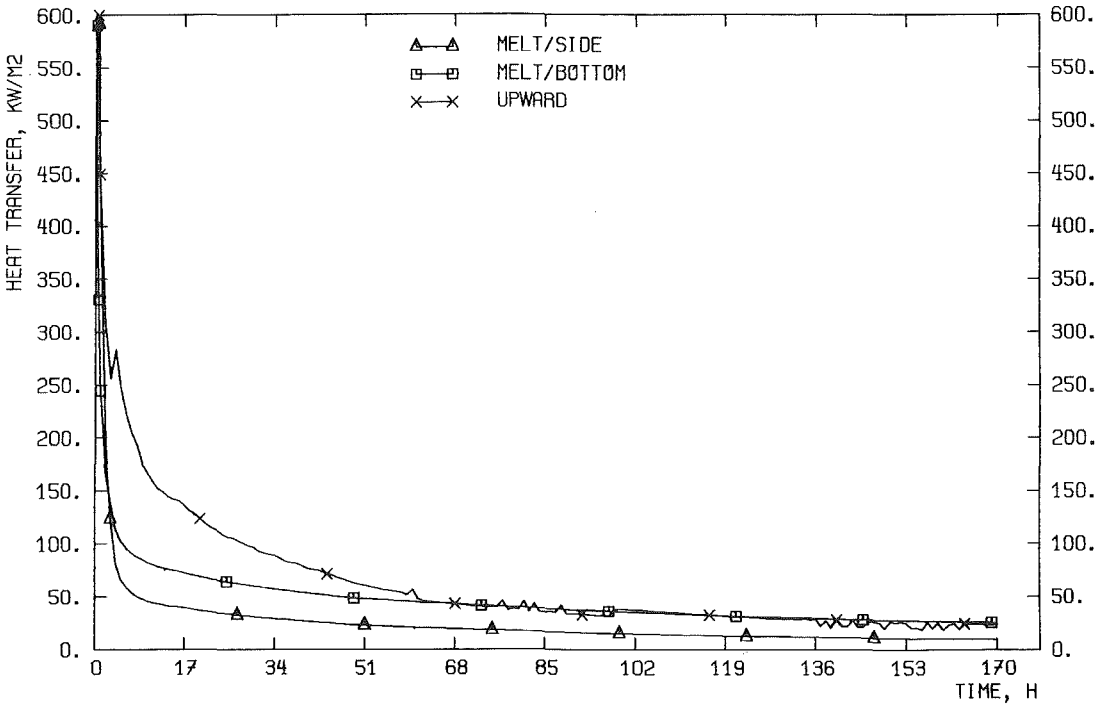


Fig. 10: PWR heat fluxes (mixed calculation).

### 2.2.2 Concrete Ablation

The erosions predicted for both melt configurations are summarized in Table 3:

| Melt Configuration | Mixed | Separated |
|---|---|---|
| Time of radial erosion of 0.9 m thick shield (hours) (time of water ingression) | 3 | 14.6 |
| Basemat penetration time (days) | 7.1 | 5.2 |
| Mass of eroded concrete (kg) | $2056 \times 10^3$ | $1730 \times 10^3$ |

Table 3: WECHSL results for PWR basemat erosion

The cavity profile of the layered calculation is given in Figure 11. In contrast to the former results [3], there is no step in the axial ablation front which corresponds to the ablation of an annulus by the oxide phase around the frozen metal layer. The WECHSL version under consideration predicts the penetration by the frozen metal layer of the 6 m thick basemat within 5.2 days instead of local break-through of the oxide melt within 4.9 days as calculated in [3]. This and the time delay of water ingression by a factor of two compared to the results of [3] are consequences of heat transfer modeling for the oxide melts described in [9]. The present WECHSL version predicts a more pronounced axial erosion and lower radial erosion rates than the version used for calculations in [3].

The cavity form for the mixed melt is shown in Figure 12. The reduced heat transfer from the oxide melt results in lower concrete erosion rates and, consequently, leads to higher melt temperatures. In the long term, however, the higher oxidic melt temperatures lead to higher heat fluxes to the concrete and, finally, to a prediction of the time of water ingression and the time of basemat penetration similar to that obtained in [3].

### 2.2.3 Chemistry and Gas Release

The oxidation times of Zr and Si are given in Table 4.

| Melt Configuration | Duration of the Oxidation Process [s] | | |
|---|---|---|---|
| | Zr Chemistry | Si Chemistry | Cr Chemistry |
| Layered | 71 | 4141 | 32965 |
| Mixed | 332 | 9655 | 22142 |

Table 4: Oxidation times

The differences in oxidation times are a reflection of the early ablation rates. The gas release rates are given in Figure 13 and Figure 14. The WECHSL code predicts either reduced gases or non-reduced gases because of complete oxidation modeling, i. e. all gases seen by metals will be reduced. Consequently, in the layered calculation there is a production of $CO_2$ and $H_2O$ coming from the decomposed concrete by the upper oxide layer (Figure 15). In the mixed calculation the characteristic changeover of the reduction of $CO_2$ occurs after 45 h and coincides with the completion of the oxidation of Fe (Fig. 14). The increase in $H_2O$ release after 14.6 h for the layered melt and after 3 h for the mixed melt is caused by sump water ingression which coincides with the radial ablation to 4.1 m.

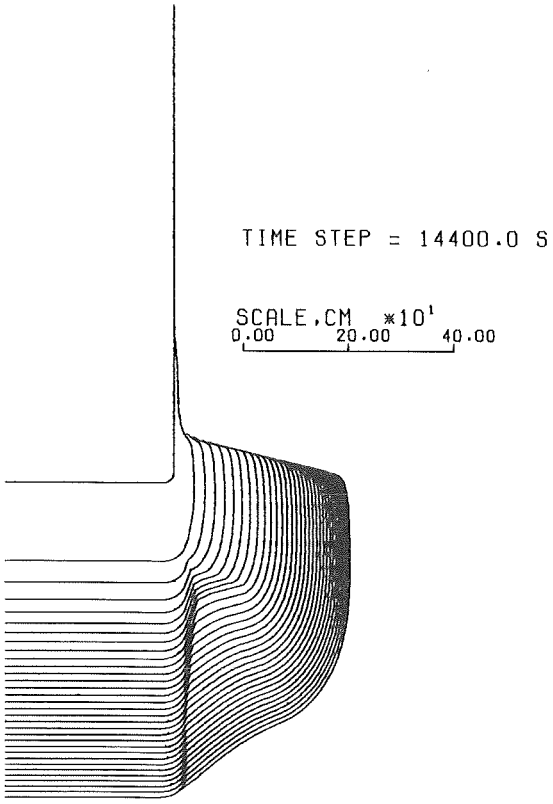


Fig. 11: PWR cavity (layered calculation).

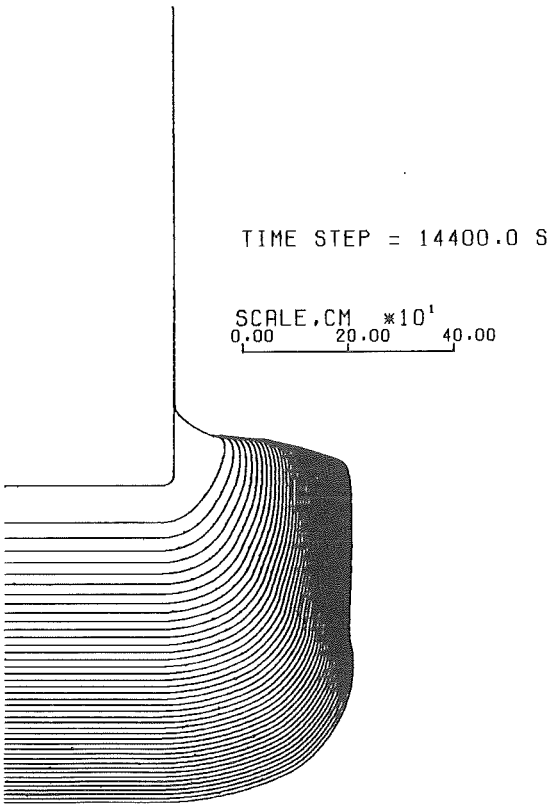


Fig. 12: PWR cavity (mixed calculation).

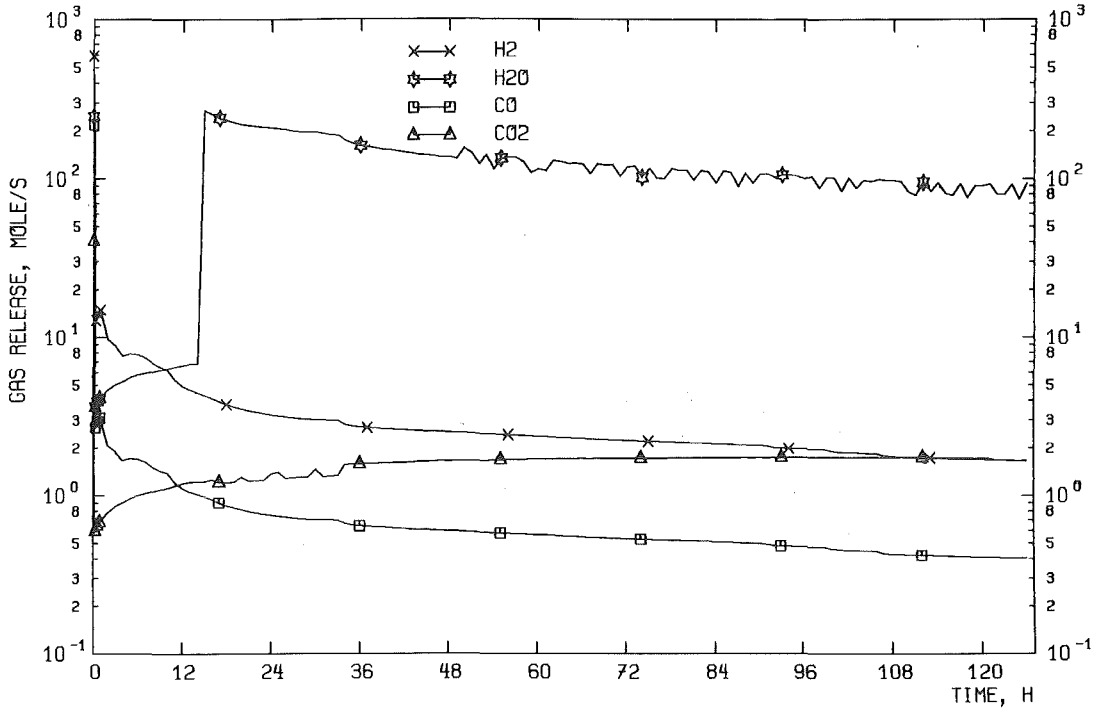


Fig. 13: PWR gas release rates (layered calculation).

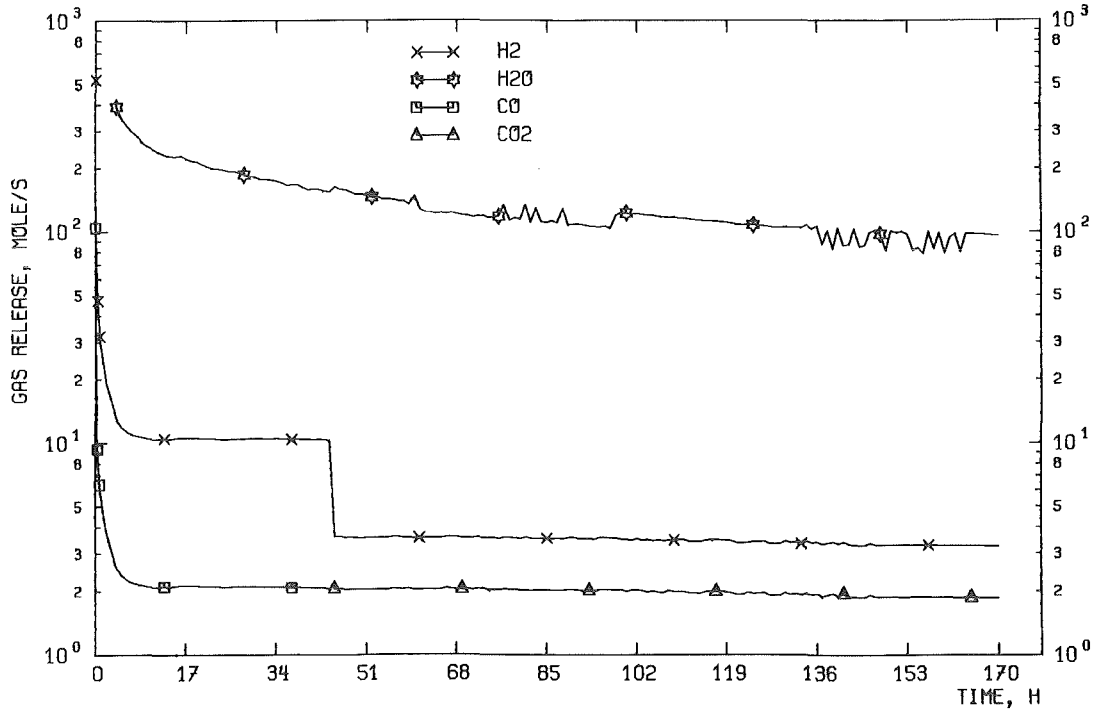


Fig. 14: PWR gas release rates (mixed calculation).

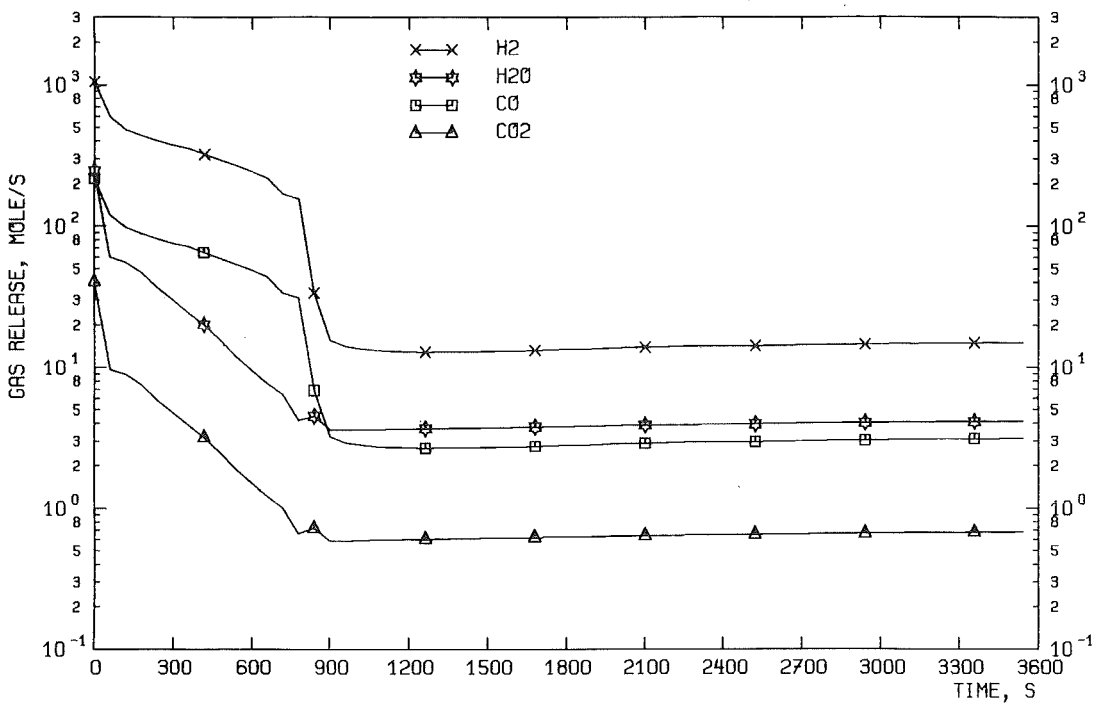


Fig. 15: PWR gas release rates (layered calculation).

### 2.2.4 Comparison of WECHSL Results for the Stratified Melt and Mixed Melt Configurations

The concrete decomposition products from basemat erosion would be incorporated quickly into the heavy oxide layer, leading to a rapid reduction in the density of that layer. If a layer structure were to be maintained, the oxide layer would relocate above the metal layer after passing through the metal layer as the difference between the densities of the two layers becomes small. Mixing and entrainment, enhanced by gas flow, would occur and it is by no means certain that the two layers would separate again. The question to be addressed is when the melt is mainly oxidic, whether or not, after mixing, the metal will separate out again into a lower layer and, if so, how quickly? If a metal layer separates out quickly, it is reasonable to use the layer structure where the metal layer is confined to the bottom of the cavity. However, if separation occurs later-on in the MCCI, or not at all, the single mixed layer model is the best assumption.

The different partition of the radial and axial heat fluxes to the concrete for both melt configurations leads to somewhat different predictions. Faster penetration of the 6 m thick basemat (within 5.2 days), lesser eroded mass of concrete and later sump water ingression (after 14.6 hours) are the main consequences of a more pronounced downward erosion and lower radial erosion rates calculated for the segregated melt. For the mixed melt configuration the basemat penetration occurs within 7.1 days and sump water ingression within only 3 hours. The total amount of released gases is related to the mass of eroded concrete, except for the evaporated sump water, and is therefore lower for the layered calculation. The long term temperatures of the oxide melt which are important to fission gas release are slightly higher during the first 2.5 days of MCCI for the layered melt configuration.

## 3. Uncertainty Analysis

Various accident sequences result in a variation of initial conditions for MCCI calculations. In the following chapters the influence of different initial conditions and different melt properties on the results of the WECHSL MCCI analysis will be analyzed.

### 3.1 Influence of the Initial Extent of Zr Oxidation

The analysis was performed on two extreme assumptions. It was assumed that the extent of Zr oxidation of the corium at the beginning of the core-concrete interaction was either 0 % or 100 %. For the reference case treated in Chapter 2, the initial oxidation of Zr was assumed to be 40 %. The corresponding cavity shapes for the layered and mixed melt configuration are given in Figures 16 and 17 and Figures 18 and 19, respectively. It can be concluded that the small extent of Zr oxidation, i.e. the release of a high amount of chemical energy due to the exothermic oxidation reactions of Zr, will influence the short time predictions of MCCI calculations. The mixed melt calculation predicts a high temperature plateau until the oxidation reaction is completed. Thereafter, the oxide melt temperature drops within about 1 hour to the level predicted for the melt containing no Zr metal (see Figure 20 and Figure 21). The short term temperature behavior for the layerd calculations is depicted in Figures 22 and 23 for the metal melt and in Figures 24 and 25 for the oxide layer which again show higher temperatures during the Zr oxidation process. Results predicted for the erosion are summarized in Table 5 (see also Figures 26-29).

For melt temperatures higher than 2200 K an additional endothermic oxidation reaction of Zr with $SiO_2$, i. e.

$$Zr + 2SiO_2 \rightarrow ZrO_2 + 2SiO_{(g)} + 4.42\ ^{kJ}/_{gZr} \qquad (1)$$

will take place which is not modeled in WECHSL. The chemical equilibrium model of the CORCON code predicts that the oxidation reaction above (Equation 1) becomes dominant at melt temperatures about 2900 K [3]. From the analysis above it is clear that inclusion of the Zr oxidation reaction given by Equation 1 would influence only the short term MCCI predictions (see [7] and [13]).

| Melt Configuration | Mixed | | Separated | |
|---|---|---|---|---|
| Initial oxidation of Zr | 0 % | 100 % | 0 % | 100 % |
| Time of radial erosion of the 0.9 m thick shield (hours) (time of water ingression) | 2.5 | 4.6 | 14.5 | 14.8 |
| Basemat penetration time (days) | 7.1 | 7.3 | 5.1 | 5.1 |
| Mass of eroded concrete (kg) | $2077 \times 10^3$ | $2042 \times 10^3$ | $1671 \times 10^3$ | $1612 \times 10^3$ |

Table 5: WECHSL results; influence of initial Zr oxidation

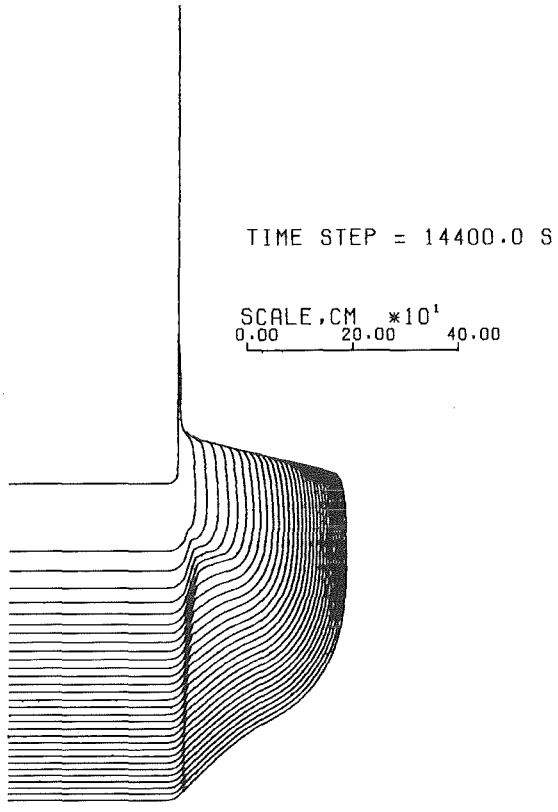


Fig. 16: PWR cavity (layered calculation, 100 % Zr preoxidation).

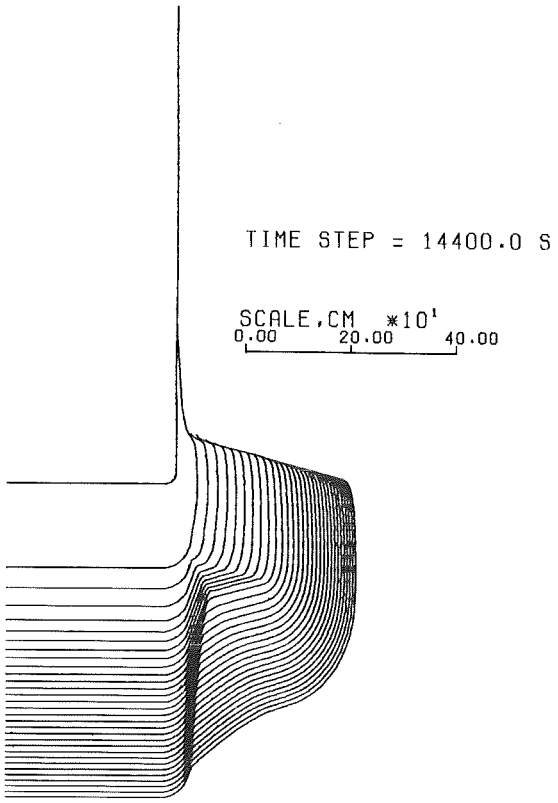


Fig. 17: PWR cavity (layered calculation, 0 % Zr preoxidation).

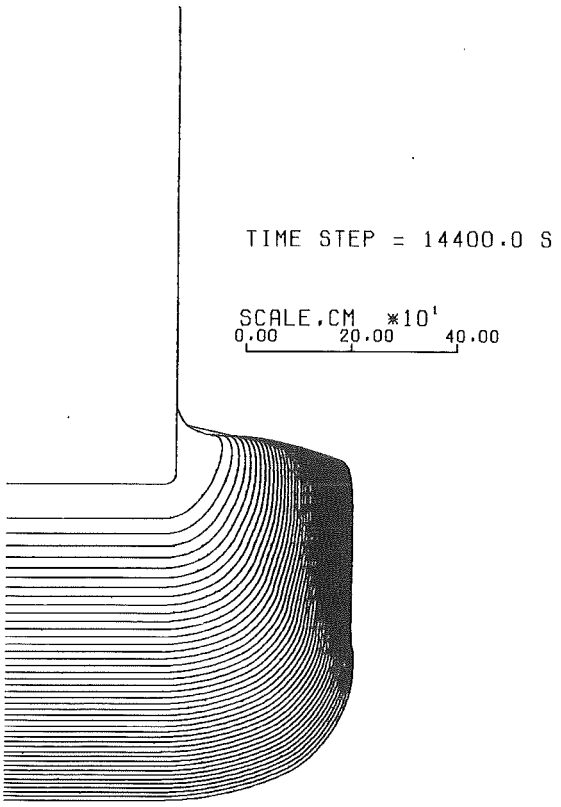


Fig. 18: PWR cavity (mixed calculation, 100 % Zr preoxidation).

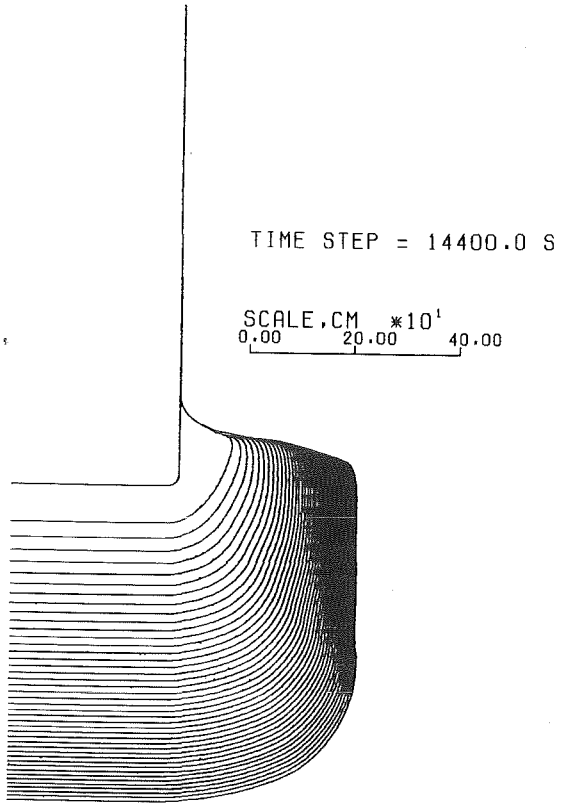


Fig. 19: PWR cavity (mixed calculation, 0 % Zr preoxidation).

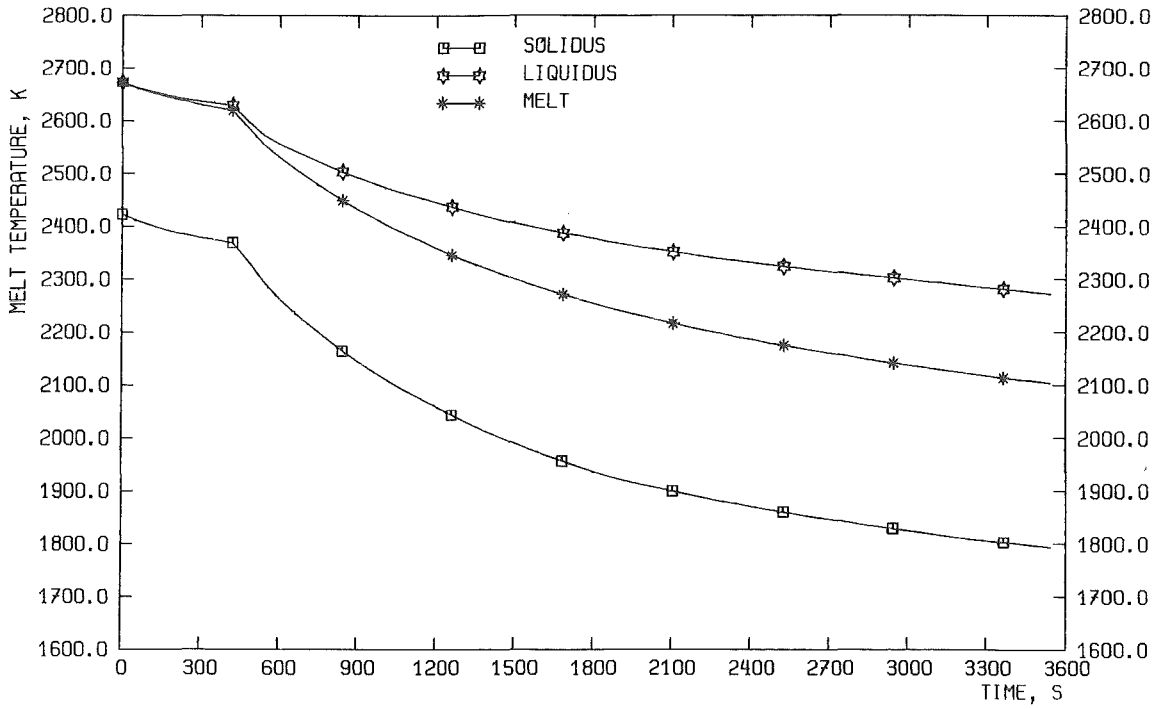


Fig. 20: PWR melt temperature (mixed calculation, 0 % Zr preoxidation).

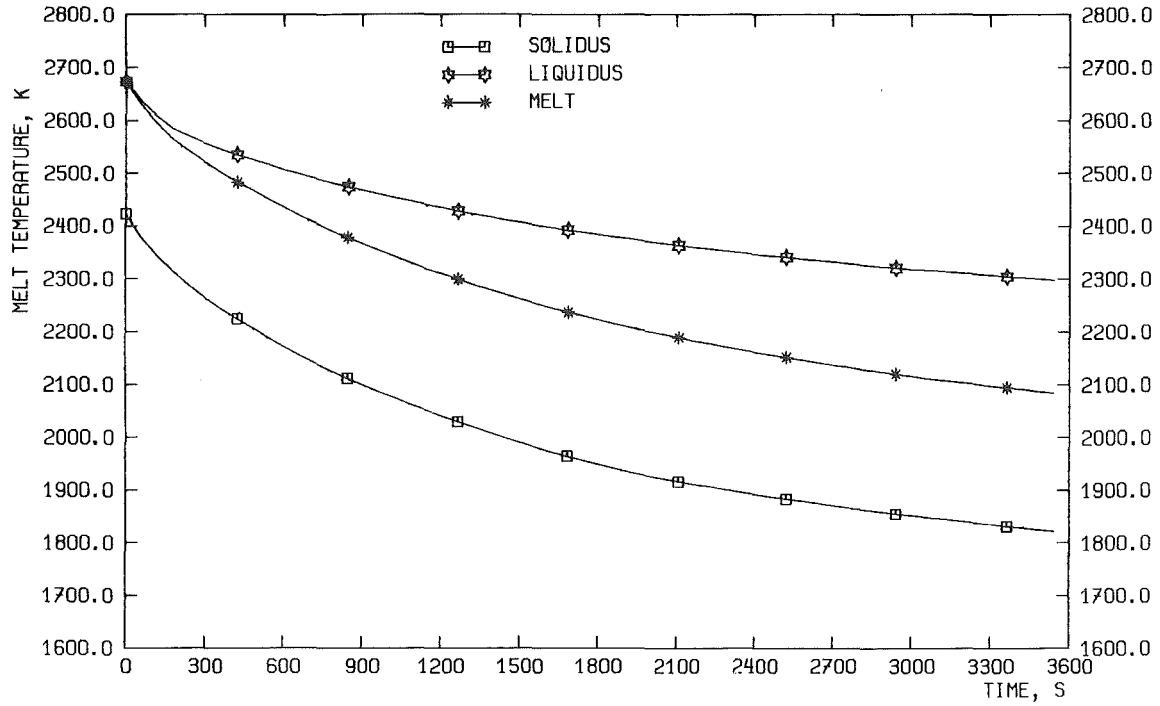


Fig. 21: PWR melt temperature (mixed calculation, 100 % Zr preoxidation).

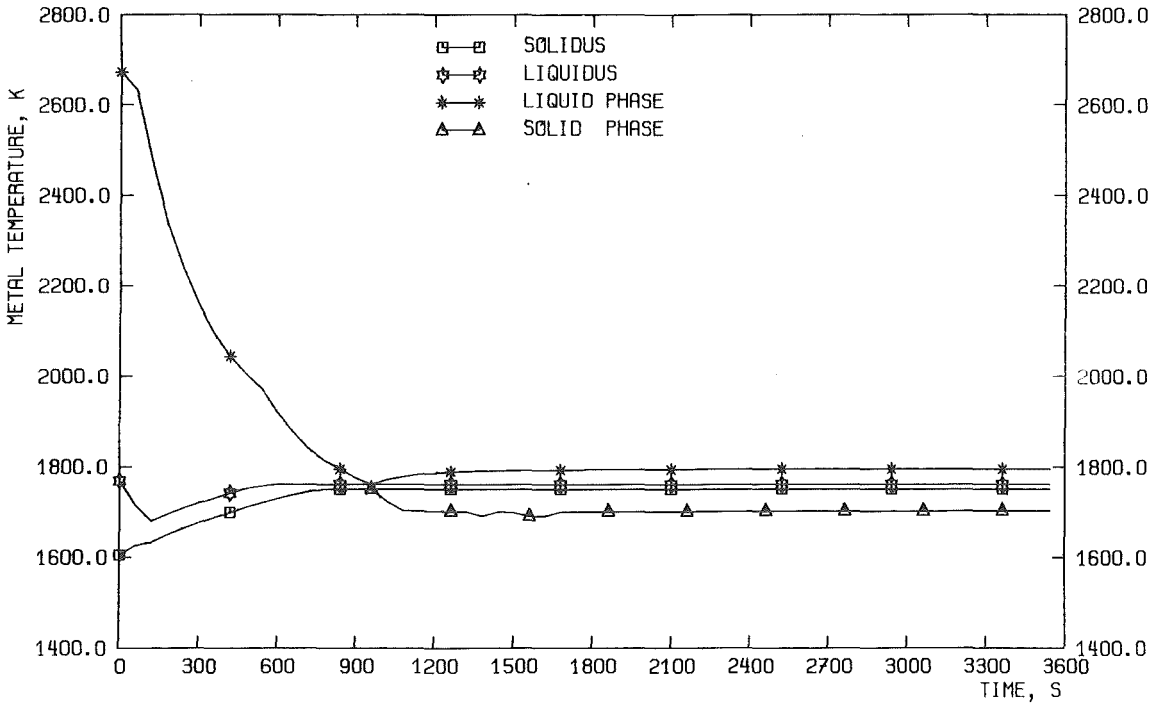


Fig. 22: PWR metallic melt temperatures
(layered calculation, 0 % Zr preoxidation).

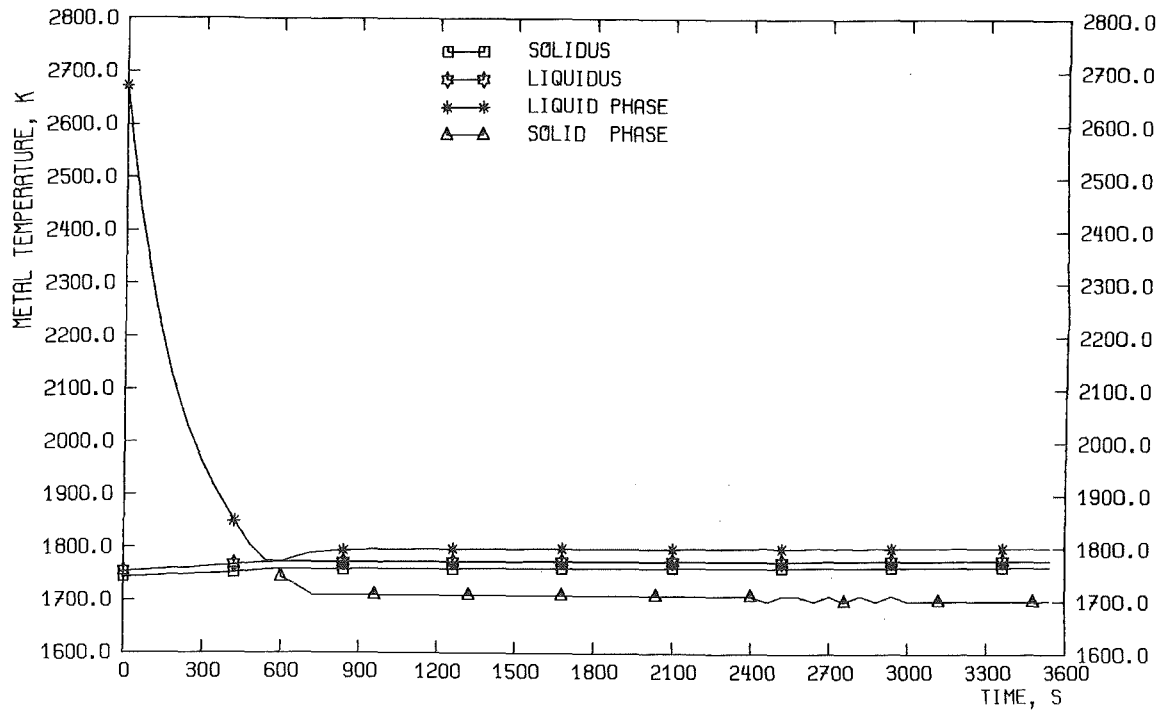


Fig. 23: PWR metal melt temperatures
(layered calculation, 100 % Zr preoxidation).

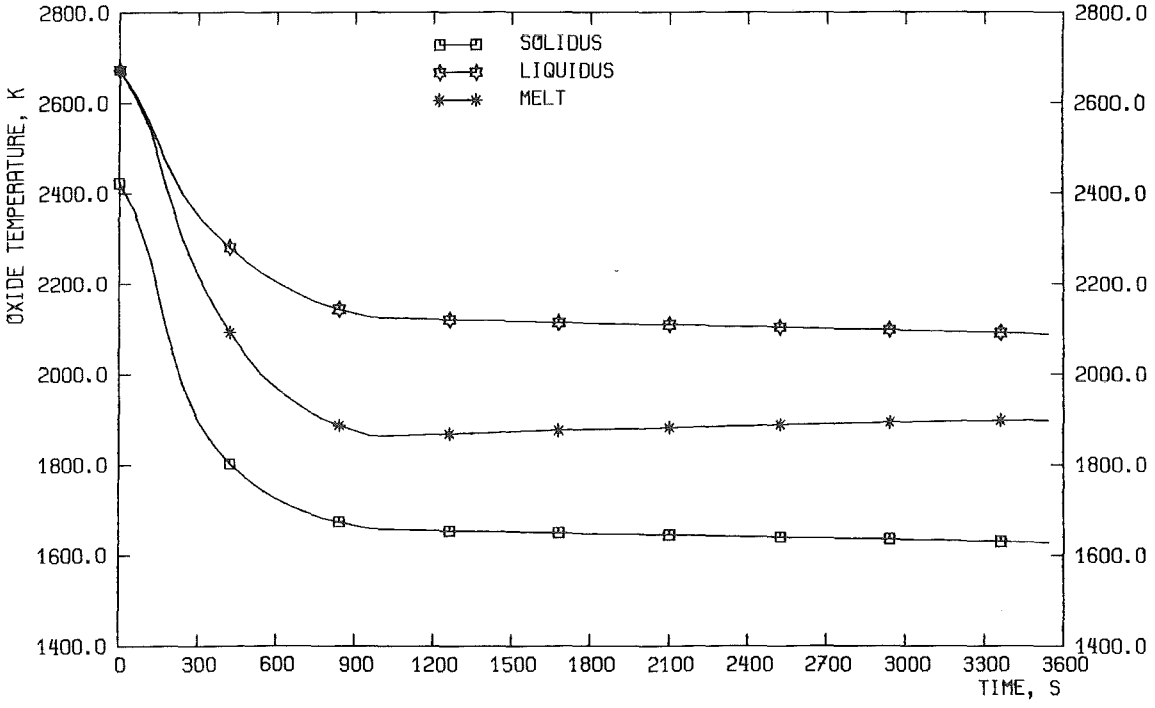


Fig. 24: PWR oxide melt temperatures
(layered calculation, 0 % Zr preoxidation).

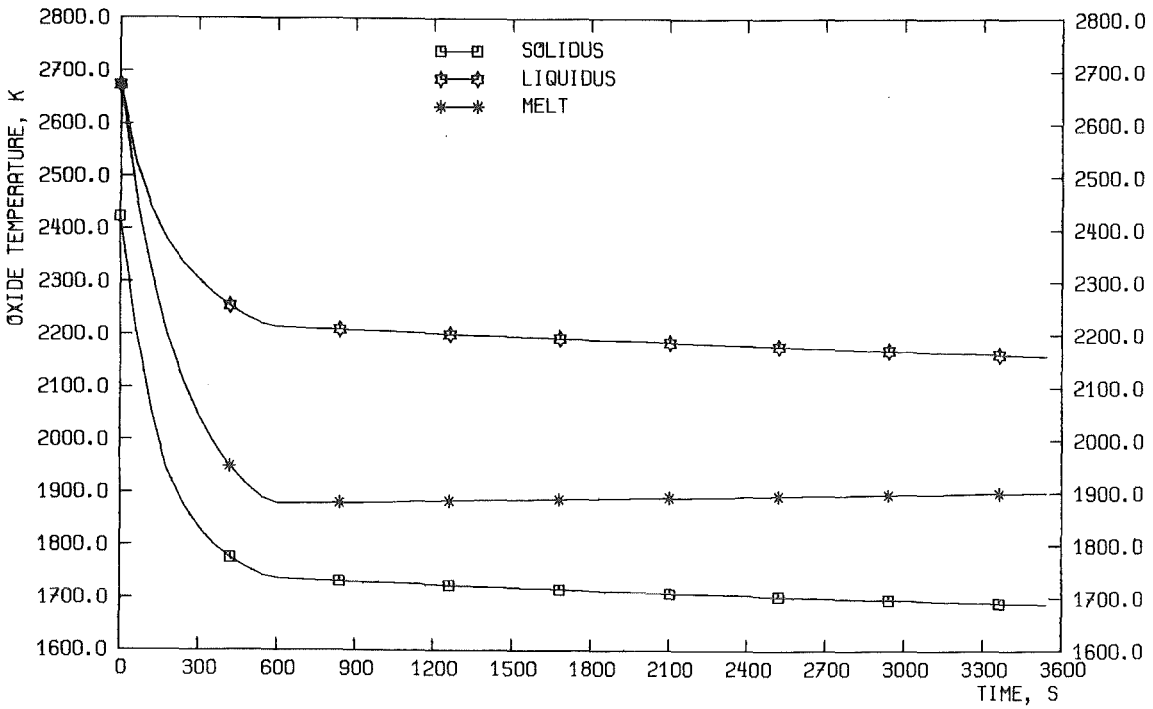


Fig. 25: PWR oxide melt temperatures
(layered calculation, 100 % Zr preoxidation).

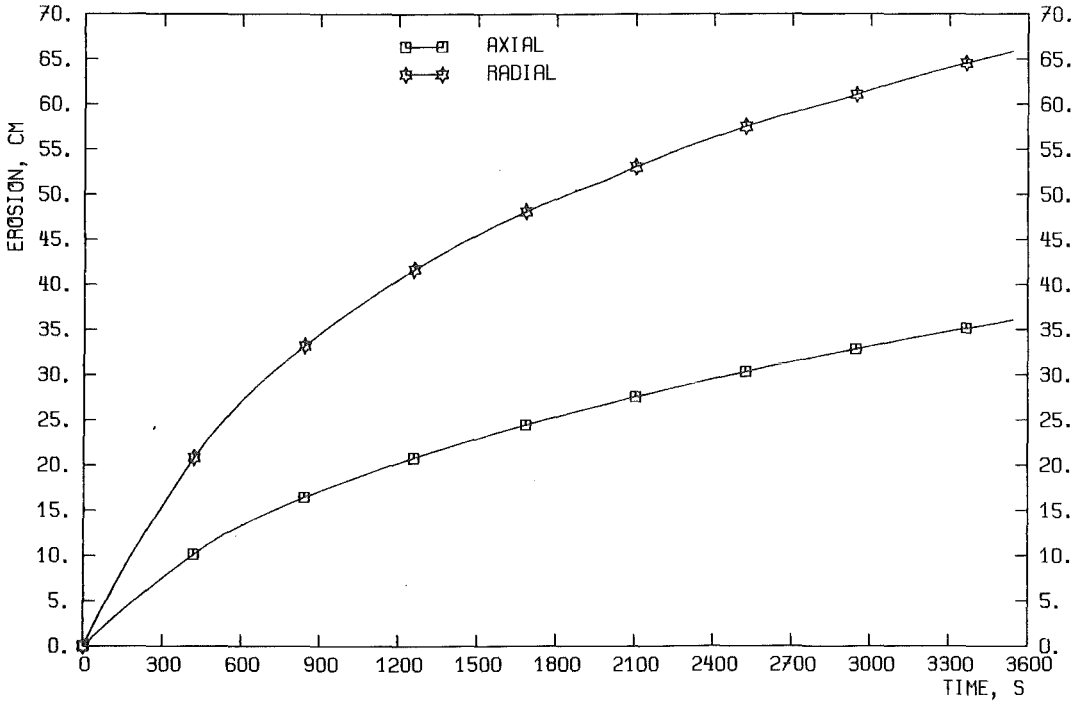


Fig. 26: PWR erosion (mixed calculation, 0 % Zr preoxidation).

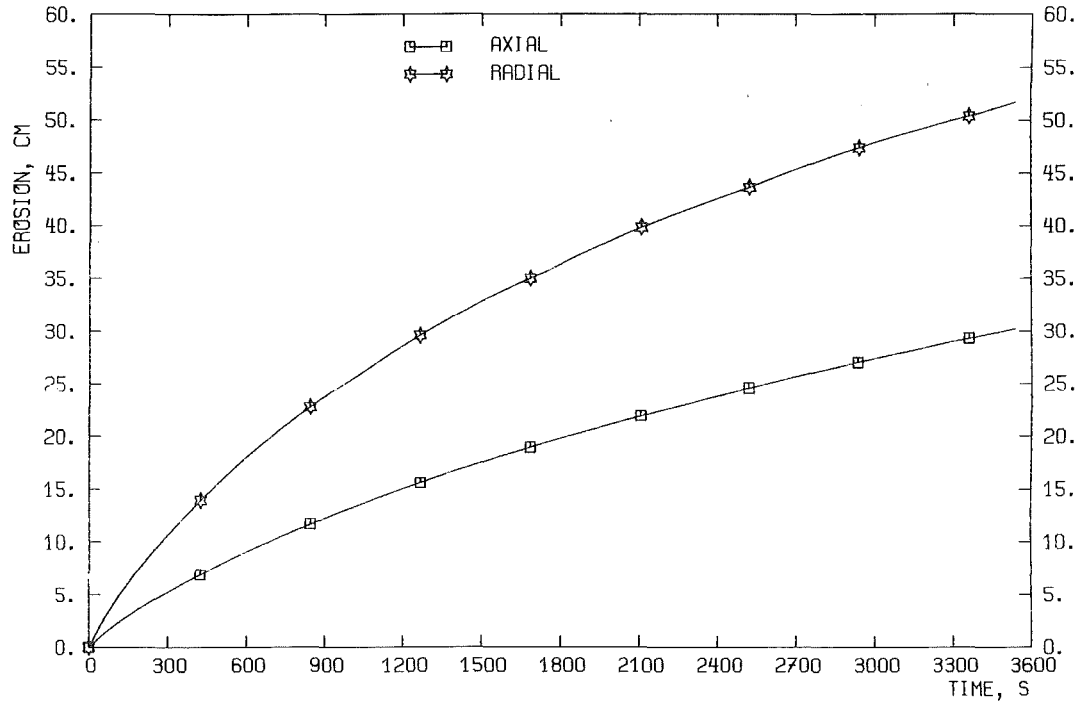


Fig. 27: PWR erosion (mixed calculation, 100 % Zr preoxidation).

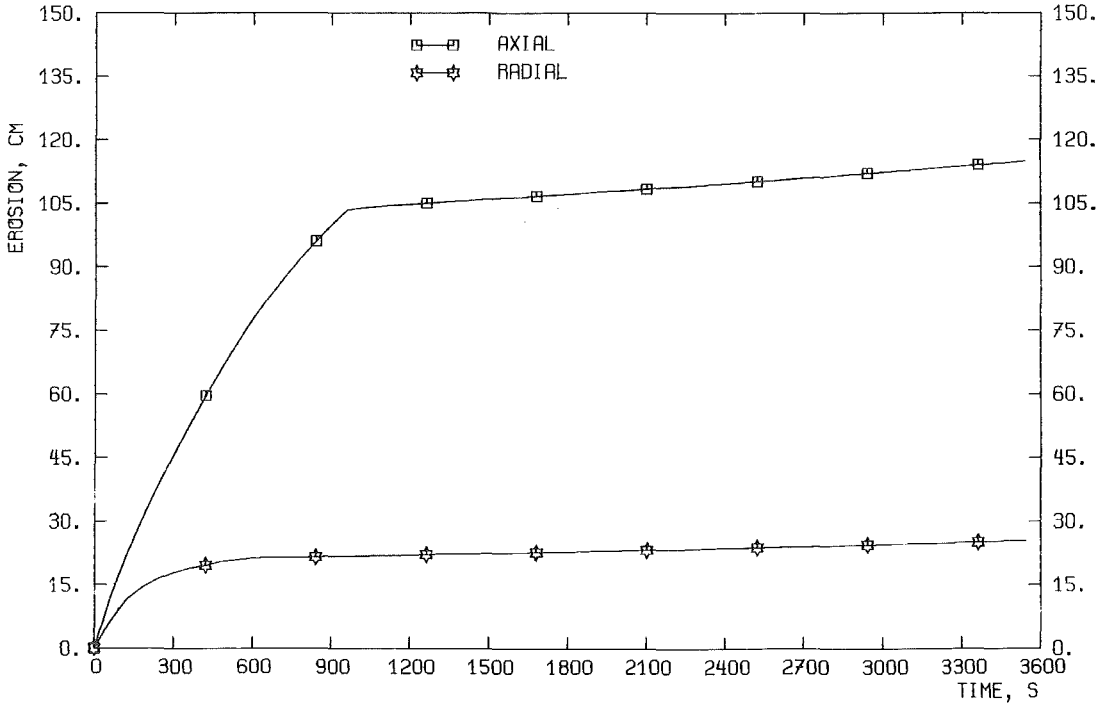


Fig. 28: PWR erosion (layered calculation, 0 % Zr preoxidation).

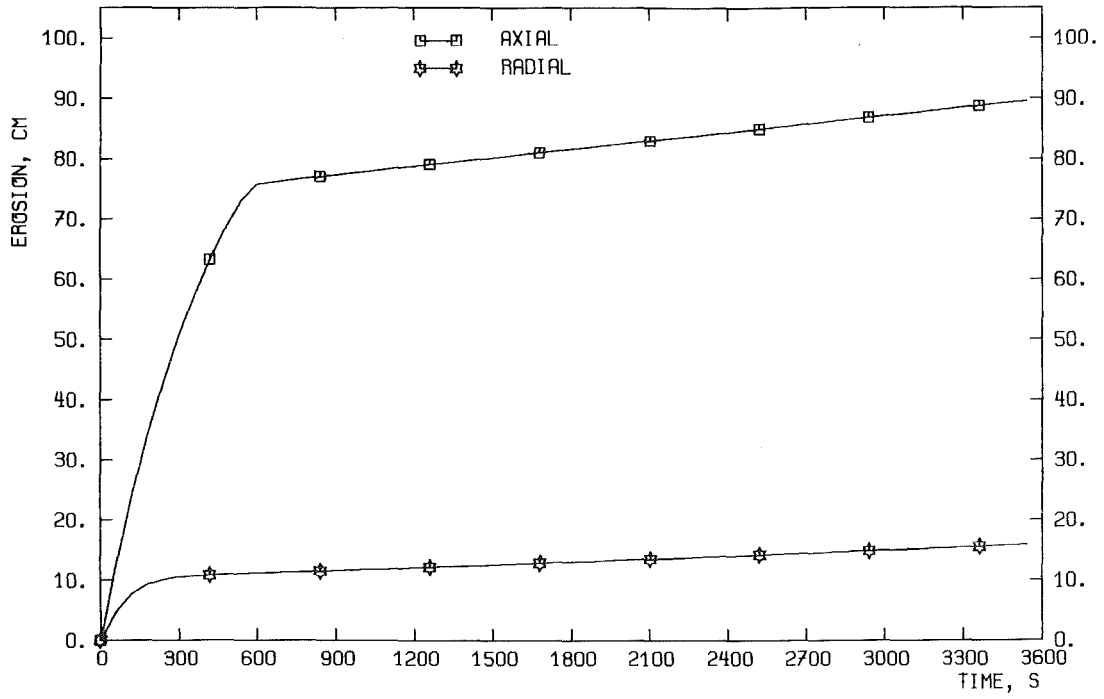


Fig. 29: PWR erosion (layered calculation, 100 % Zr preoxidation).

## 3.2 Influence of High Initial Melt Temperatures

Calculations with an initial melt temperature of 3000 K were performed for both melt configurations. In either case only the short term WECHSL predictions are influenced by the variation of the initial temperature. The mixed melt calculation predicts a drop within about 900 s of the melt temperature to the level predicted for the standard case with an initial temperature of 2673 K (Figure 3) (see Figure 30). For the layered calculation this is predicted to occur within only 100s (Figures 31 and 32). Higher erosion rates in these time periods cause higher $H_2$ release rates. Results for the erosion are given in the following Table 6. These results differ only slightly from those obtained for the reference case (Table 3).

| Melt Configuration | Mixed | Separated |
|---|---|---|
| Time of radial erosion of the 0.9 thick shield (hours) Time of water ingression | 2.4 | 13.4 |
| Basemat penetration time (days) | 7.2 | 5.4 |
| Mass of eroded concrete (kg) | 2077 x $10^3$ | 1746 x $10^3$ |

Table 6: WECHSL results, influence of higher initial temperature of the corium melt

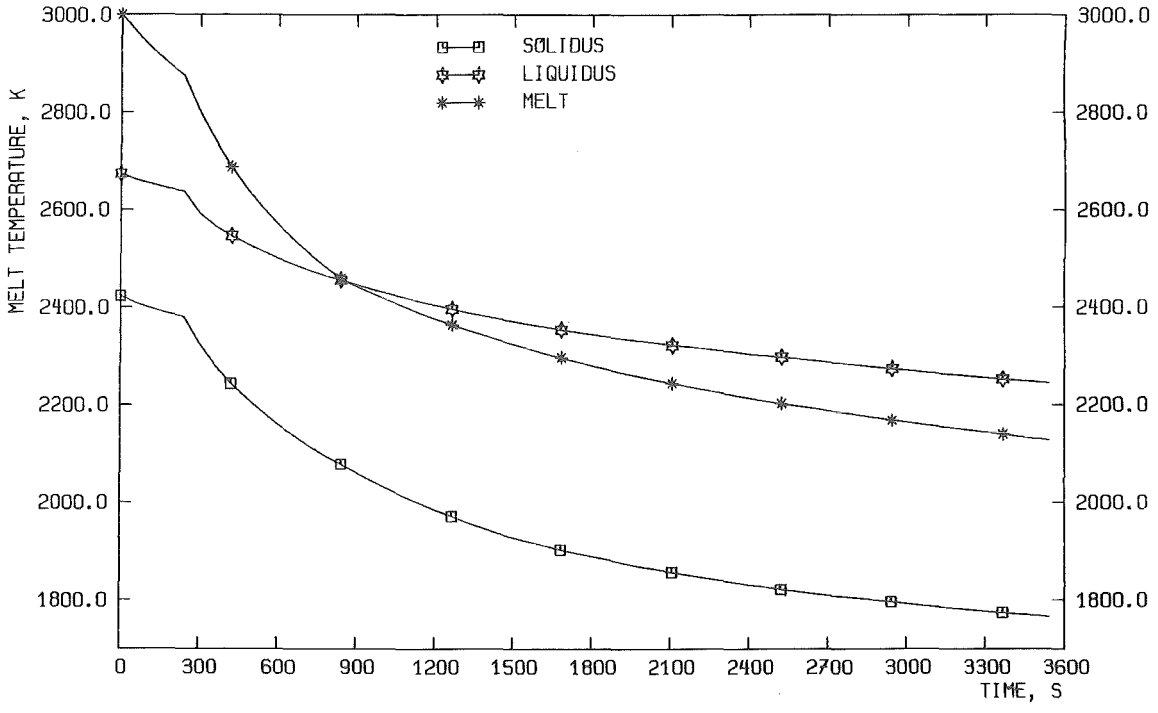


Fig. 30: PWR melt temperatures (mixed calculation, initial melt temperature 3000 K).

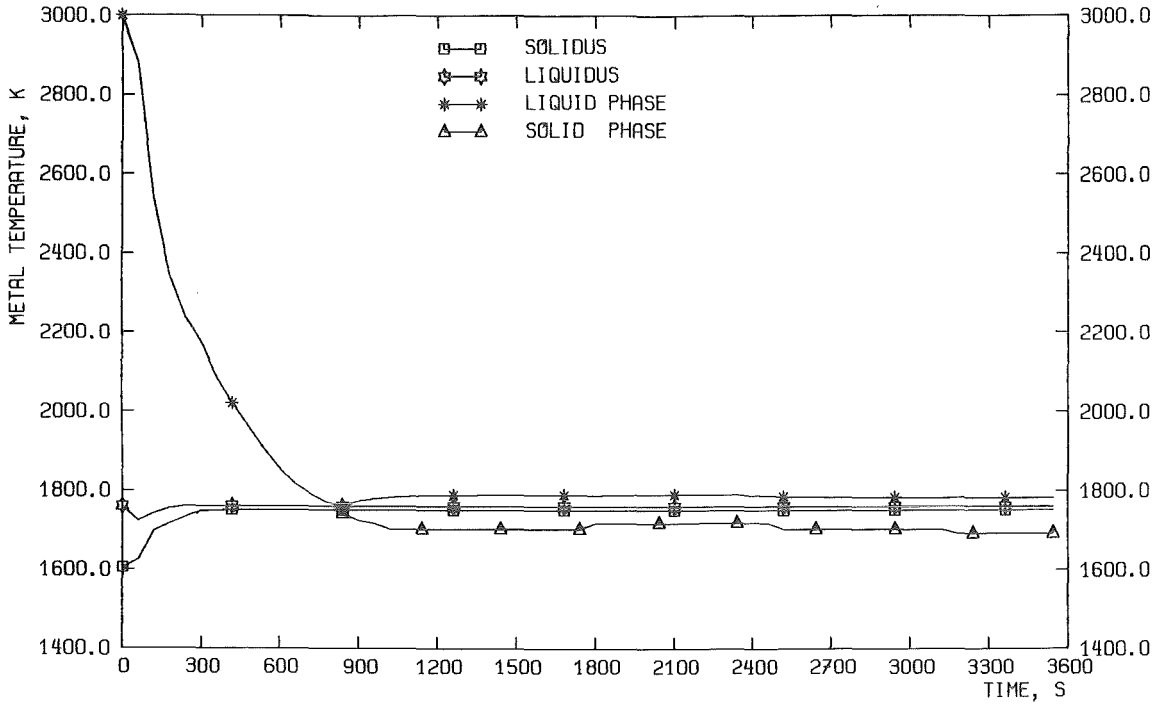


Fig. 31: PWR metal temperatures
(layered calculation, initial melt temperature 3000 K).

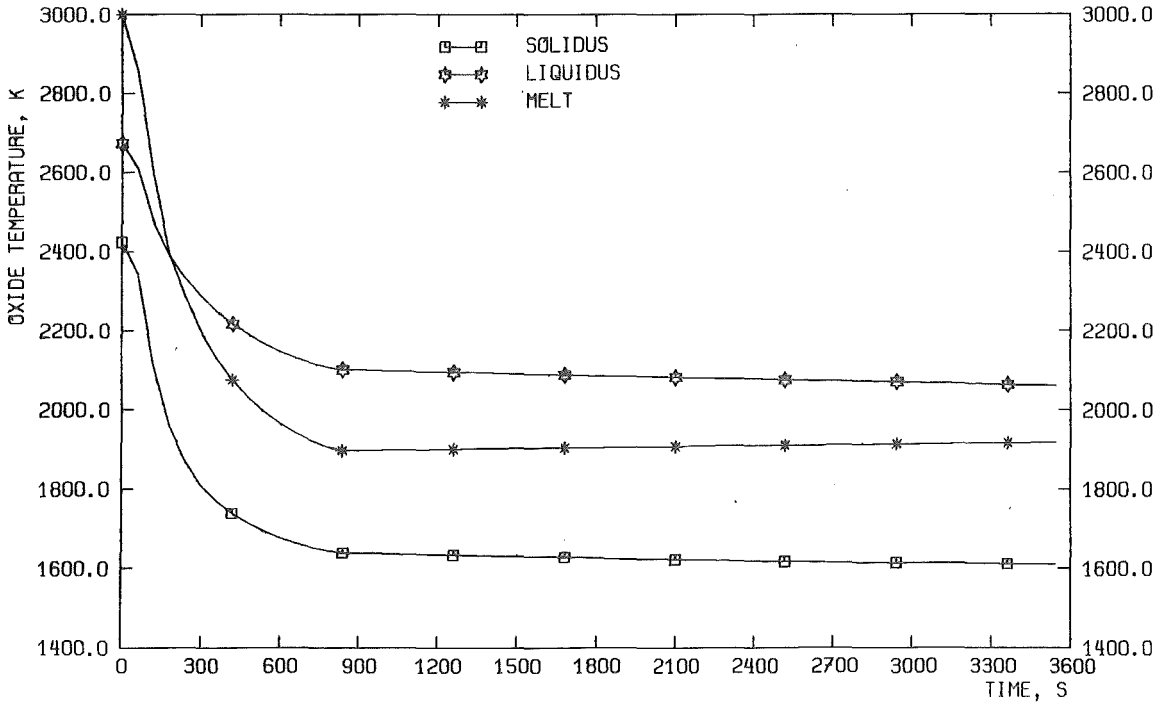


Fig. 32: PWR oxide melt temperatures
(layered calculation, initial melt temperature 3000 K).

## 3.3. Influence of Melt Properties

The solidus and liquidus temperatures are not well known for oxide corium melts. It is possible that the solidus temperature is very close to that of the concrete for all but very low fractions of concrete decomposition products in the melt. The question arises of the meaning of the "solidus" for melt calculations. A reasonable definition of "solidus" in the present context is that it is used to describe the temperature below which conduction is the sole heat transport mechanism available. Then, the so-called softening temperature may be used which describes the point at which the viscosity of a melt reaches $10^7$ Pa · s [14]. Thus, if a good model of melt viscosity was available, the softening temperature would be a good choice for the "solidus." However, currently available viscosity models do not agree very well with experimental data which, in addition, have a broad range of uncertainties.

### 3.3.1 Variation of the Solidus Temperature of Oxide Melts

Two calculations were performed for a mixed melt configuration, one on the assumption of a high solidus temperature and one using a low solidus temperature. In accordance with [15], the solidus temperature of the oxide phase was modeled to drop rapidly as concrete decomposition products are incorporated into the melt, approaching the concrete solidus at only 20 weight per cent of concrete oxides (Figure 33). The high solidus temperatures were used to simulate extremely high softening temperatures (Figure 34).

The calculations performed show only a weak influence of the solidus temperature of the oxide melt on the WECHSL results. The behavior of the temperatures of the melt during the first hour of MCCI are shown in Figures 33 and 34. The faster basemat penetration (6.6 days) predicted for the high solidus temperature is a consequence of the reduction of heat losses from the top of the melt which is due to formation of a thicker crust than calculated for the melt with a low solidus temperature of the oxide melt. In this case, basemat penetration was predicted to occur within 7.3 days (see Table7).

| Melt Configuration | Mixed | |
|---|---|---|
| Solidus temperature | High | Low |
| Time of radial erosion of the 0.9 m thick shield (hours) (Time of water ingression) | 2.6 | 3.2 |
| Basemat penetration time (days) | 6.6 | 7.3 |
| Mass of eroded concrete (kg) | 2126 x $10^3$ | 2028 x $10^3$ |

Table 7: WECHSL results for different solidus temperatures of the melt

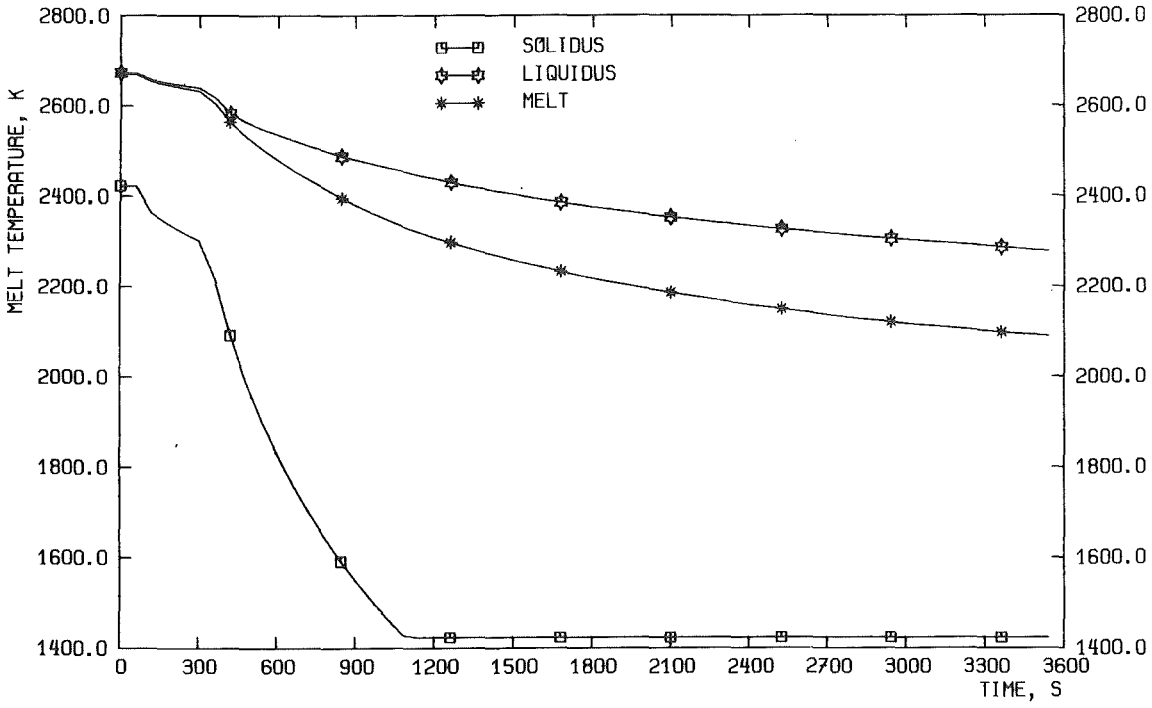


Fig. 33: PWR melt temperatures (mixed calculation, low solidus temperature).

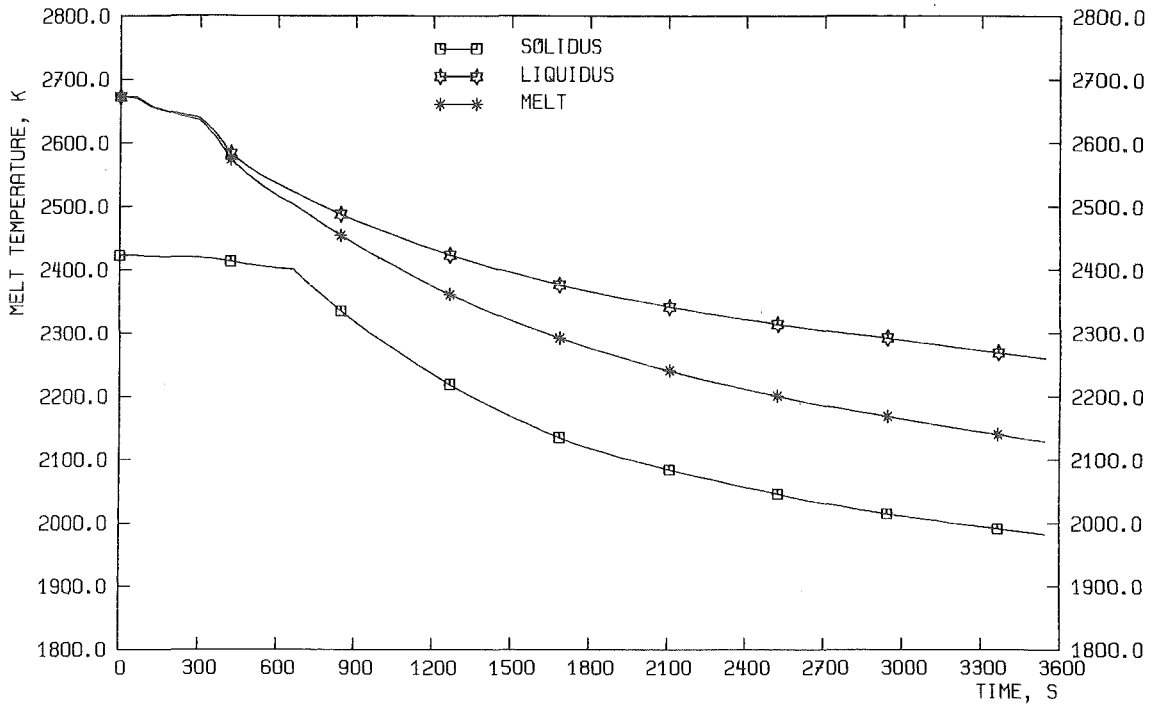


Fig. 34: PWR melt temperatures (mixed calculation, high solidus temperature).

### 3.3.2 Variation of the Viscosity of Oxide Melts

The values of the viscosity recently determined by Roche et al. [15] exceed by about three orders of magnitude the values predicted by the improved viscosity model in WECHSL [9]. The effect of such high oxide melt viscosities was investigated by means of WECHSL calculations with viscosities multiplied by a factor $10^3$.

The cavity shape with a less pronounced radial erosion than in the standard case (Figure 12) is shown in Figure 35. The typical erosion times are listed in Table 8. The much smaller heat fluxes (especially the radial heat fluxes) to the concrete at the beginning of the melt-concrete interaction (Figure 36), compared to those calculated for the standard case (Figure 37), leads to high melt temperatures (Figure 38) which are 200 K to 300 K higher than predicted in Figure 5. The lower content of $SiO_2$ in the melt due to less eroded concrete mass together with the high melt temperatures yields viscosity values which are only 20 to 100 times higher than predicted by WECHSL for the standard case. The heat transfer models in WECHSL show a dependence on viscosity of the partition of radial and axial heat fluxes to the concrete. A higher melt viscosity leads to a greater ratio of the axial

heat flux to the radial heat flux. Oxide melts with low viscosities give rise to more equipartitioned heat fluxes to the concrete. An interplay of melt temperatures and heat flux partition results in the long term erosion behavior summarized in Table 8 for this kind of WECHSL simulations. It can be seen that the time for needed basemat penetration is reduced from 7.1 to 5.5 days for the highest melt viscosity. This is a remarkably little influence of the increase in viscosity.

| Melt Configuration | Mixed | | |
|---|---|---|---|
| Viscosity increase by a factor | $10^3$ | $10^2$ | 10 |
| Time of radial erosion of the 0.9 m thick shield (hours) (Time of water ingression) | 13.9 | 9.4 | 5.2 |
| Basemat penetration time | 5.5 | 5.7 | 6.2 |
| Mass of eroded concrete (kg) | $1768 \times 10^3$ | $1853 \times 10^3$ | $1962 \times 10^3$ |

Table 8: WECHSL results for higher viscosities of the oxide melt

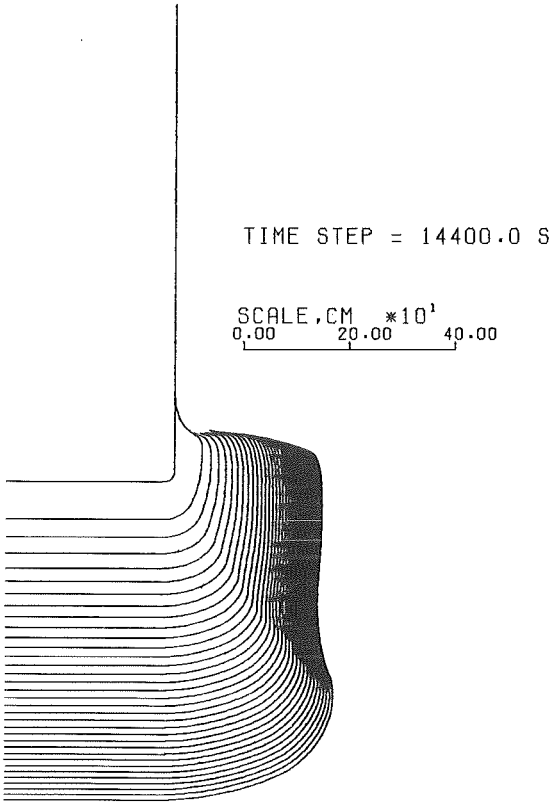


Fig. 35: PWR cavity (mixed calculation; viscosity increased by a factor $10^3$).

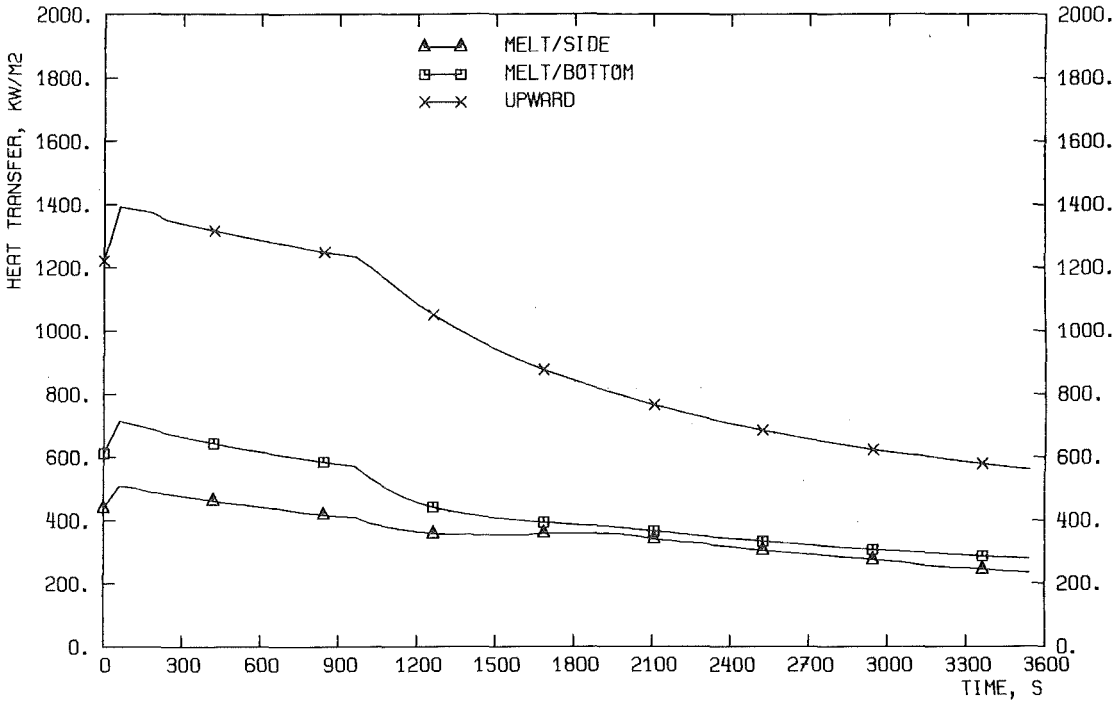


Fig. 36: PWR heat fluxes (mixed calculation, oxide viscosity increased by a factor $10^3$).

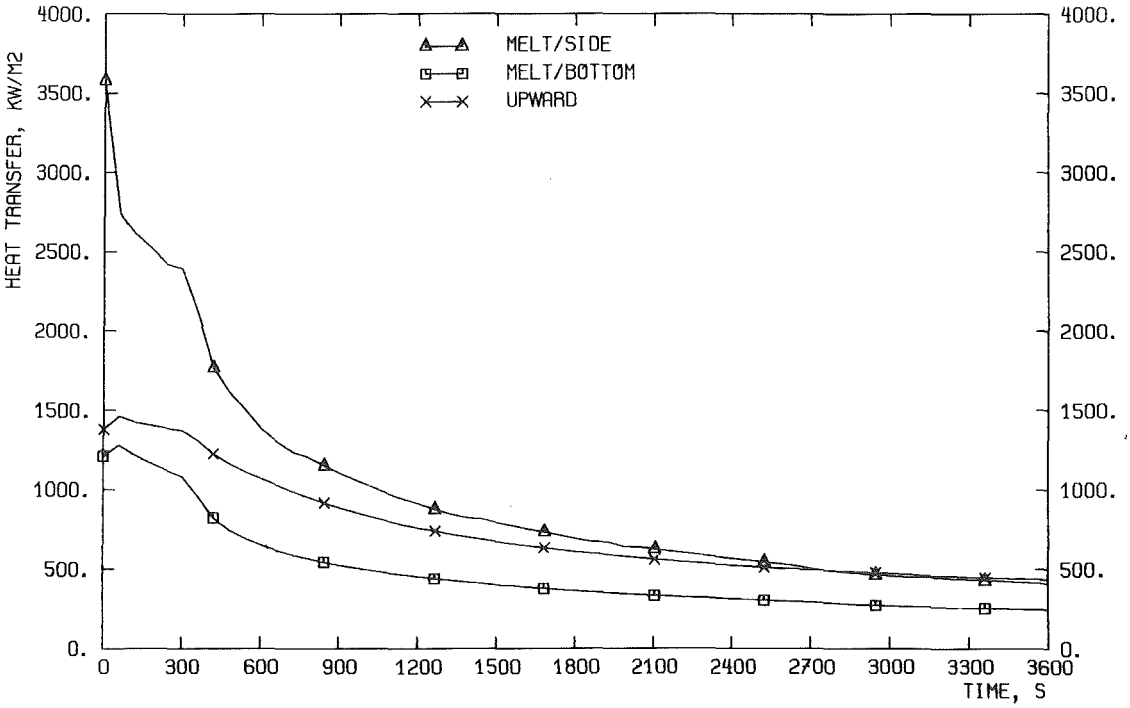


Fig. 37: PWR heat fluxes (mixed calculation, standard oxide viscosity).

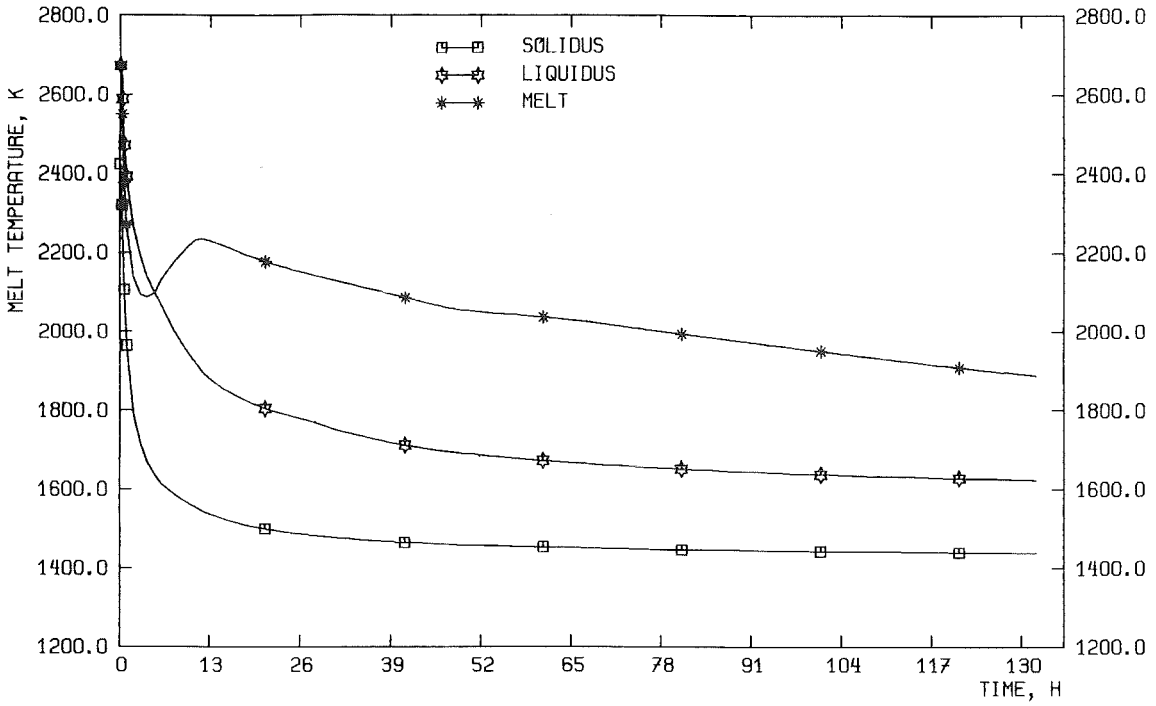


Fig. 38: PWR melt temperatures
(mixed calculation; viscosity increased by a factor $10^3$).

### 3.3.3 Influence of Thermal Conductivity Change in the Solid Phase

According to the Franz-Wiedmann-Lorenz relation, the ratio of the thermal conductivities of the solid phase to the liquid phase for metals is approximately equal to 2 at the solidus/liquidus point. The void fraction caused by gases released from the decomposing concrete will lead to a porous oxidic crust. Hence, the thermal conductivity of the surface crust will be lower compared to that of the liquid oxide. In the PWR layered calculation performed in [16] the thermal conductivity of the oxidic crust was assumed to be 0.5 times the value of the thermal conductivity of the liquid phase. It was shown that the higher thermal conductivity of a crust leads to a higher heat flux and a faster crust growth. Consequently, higher erosion rates and ensuing higher gas release rates as well as faster penetration of the concrete basemat are predicted. However, predictions of the time of basemat meltthrough differed only by about 20 %. In addition, the higher thermal conductivity gives rise to a lower mean temperature of the melt. The maximum difference for the metal melt is about 50 K, for the oxidic phase the difference does not exceed 20 K.

### 3.4 Influence of Heat Conduction in the Concrete Basemat

The concrete ablation concept in WECHSL is based on a quasi-stationary model which is characterized by the concrete ablation temperature and the concrete decomposition enthalpy neglecting transient heat conduction in the solid concrete. In order to assess the influence of heat conduction in the concrete on WECHSL MCCI results, an analysis by means of a stand-alone code was performed. Due to the poor thermal conductivity of the concrete, the quasi-stationary model in WECHSL overpredicts by about 14 % the global concrete erosion for the standard PWR (for details see [17]). Thus, it can be concluded that the quasi-stationary concrete ablation model is an adequate model for reactor accident analyses.

## 4. BWR Accident Scenario

For the sake of completeness, MCCI WECHSL calculations for a BWR with a large radius of the cavity will be presented.

### 4.1 Description of the Scenario

The low pressure accident sequence in a BWR leads to a corium inventory at the start of the MCCI which is shown in Table 9. The corium melt contains a considerably higher amount of $UO_2$ and Zr although the reactor power is the same as the power of the PWR described above. The initial melt temperature is estimated at 2673 K. The reactor cavity of the initial radius of 7 m and the basemat with a thickness of 2 m consists of a siliceous type of concrete as shown in Table2.

| Melt Constituent | Mass [kg] |
|---|---|
| Fe | $7.3 \times 10^4$ |
| Zr | $5.67 \times 10^4$ |
| Cr | $1.1 \times 10^4$ |
| Ni | $6.4 \times 10^3$ |
| $UO_2$ | $1.77 \times 10^5$ |
| $ZrO_2$ | $3.83 \times 10^4$ |

Table 9: Corium inventory in a BWR accident

## 4.2 WECHSL Results

In additon to the mixed layer calculation in [3] a calculation with the layered melt configuration was performed.

### 4.2.1 Temperature, Crust Growth and Heat Transfer

In both calculations there is a rapid fall in the melt temperatures (Figure 39 and Figures 40 - 41). The predicted plateau of the long term oxide melt temperatures is located about 100 K below the liquidus temperature for the mixed melt configuration (Figure 42) and about 50 K below the liquidus temperature for the layered configuration (Figure 43). The formation of the crust at the bottom of the metal layer starts at about 750 s after beginning of the interaction. Complete solidification takes place after 2 hours. There is no flooding of the BWR core melt surface and, consequently, a slower crust growth at the top of the melt (Figures 44 - 45). The long term heat flux distribution is similar for both BWR calculations and given in Figure 46 for the mixed melt.

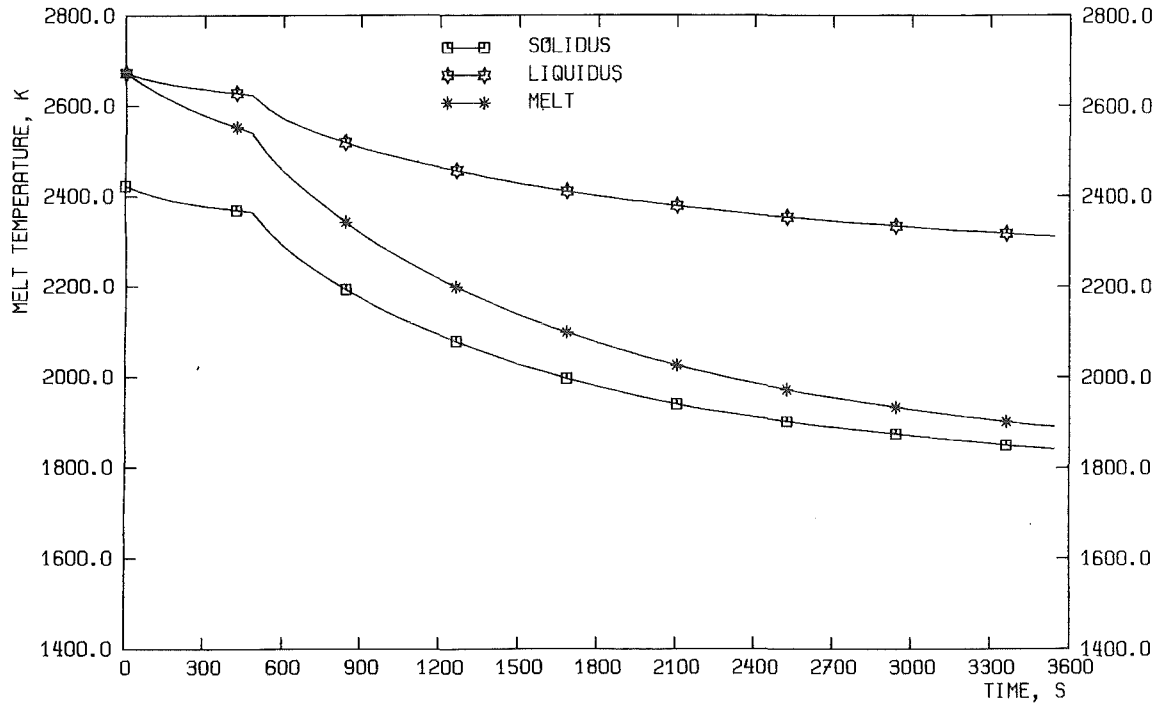


Fig. 39: BWR melt temperatures (mixed calculation).

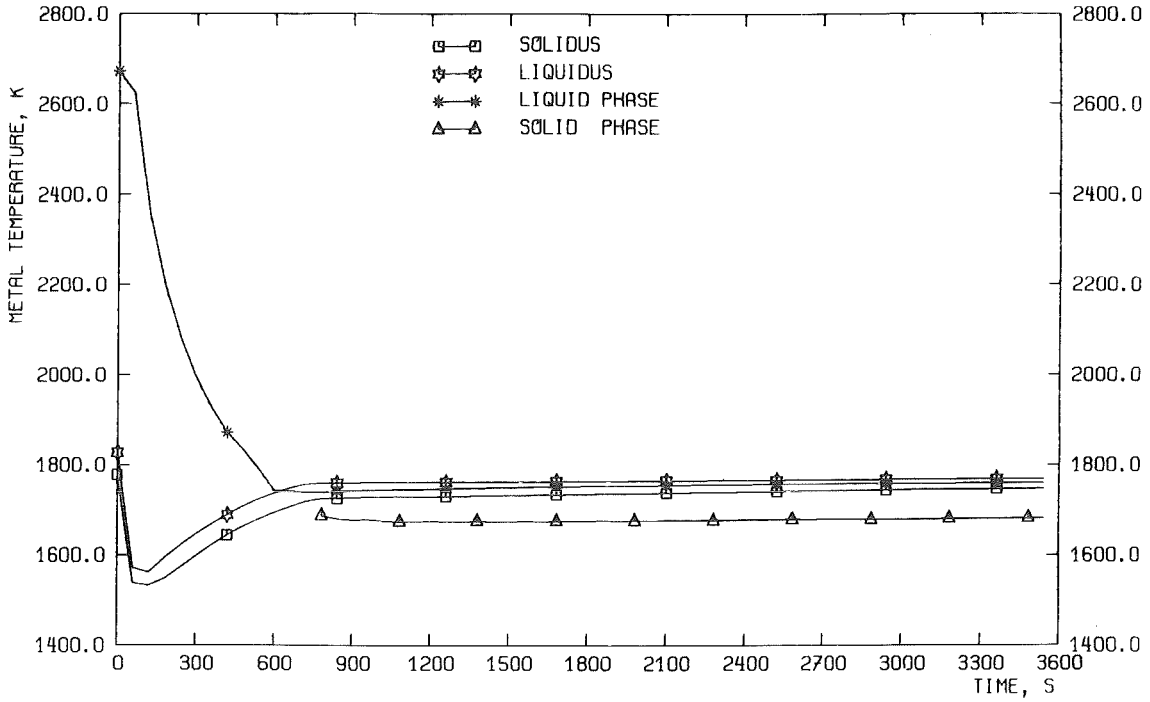


Fig. 40: BWR metal melt temperatures (layered calculation).

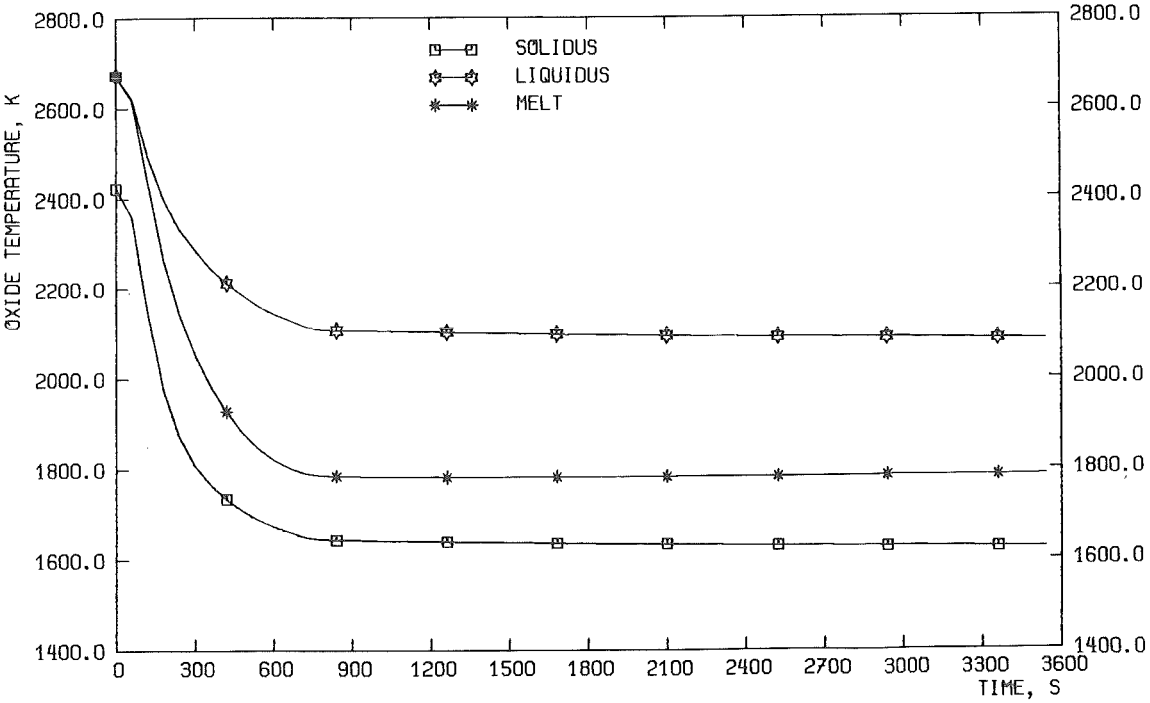


Fig. 41: BWR oxide melt temperatures (layered calculation).

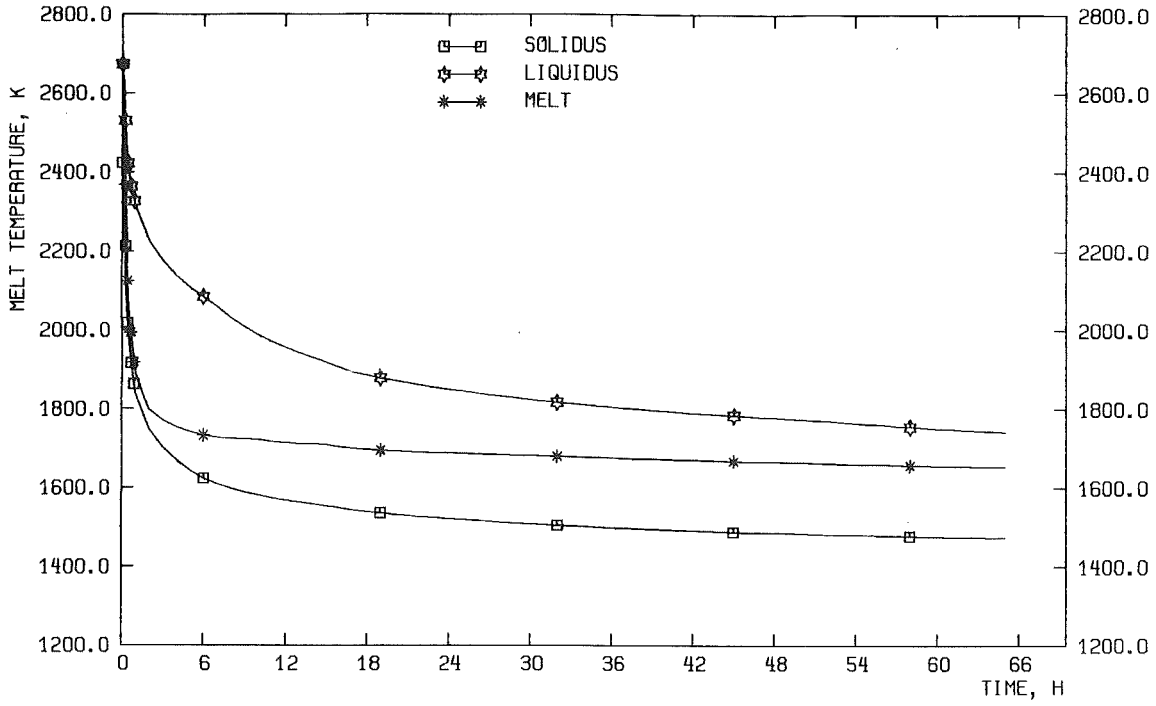


Fig. 42: BWR melt temperatures (mixed calculation).

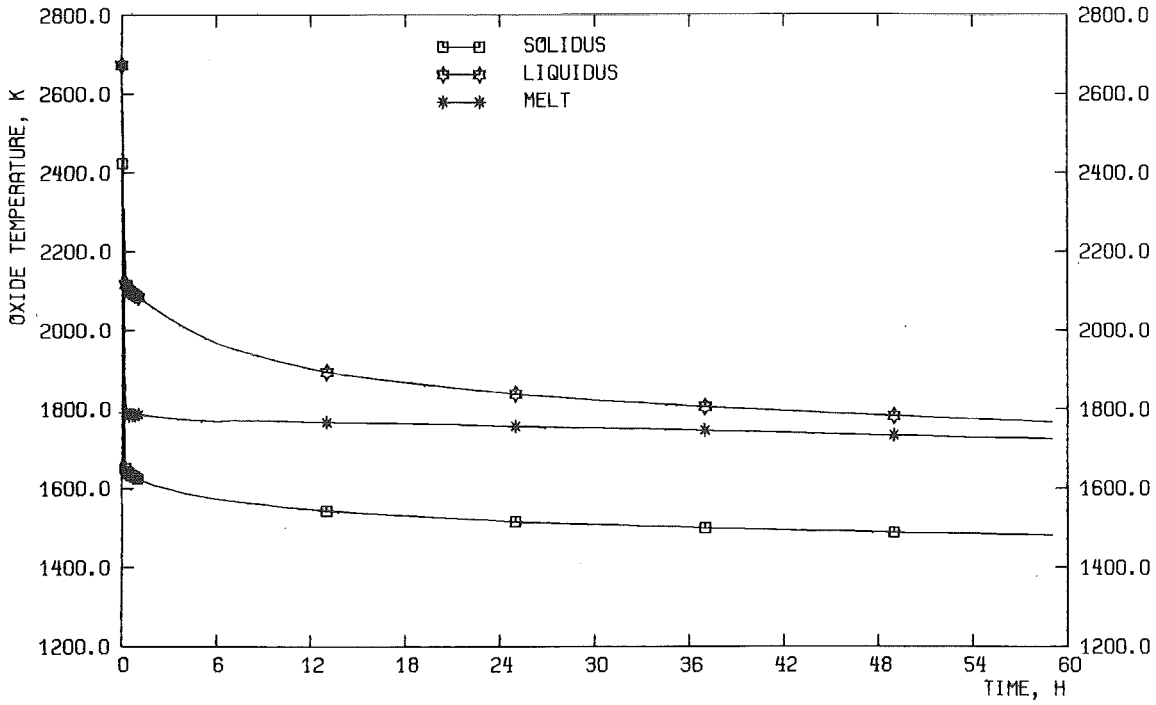


Fig. 43: BWR oxide melt temperatures (layered calculation).

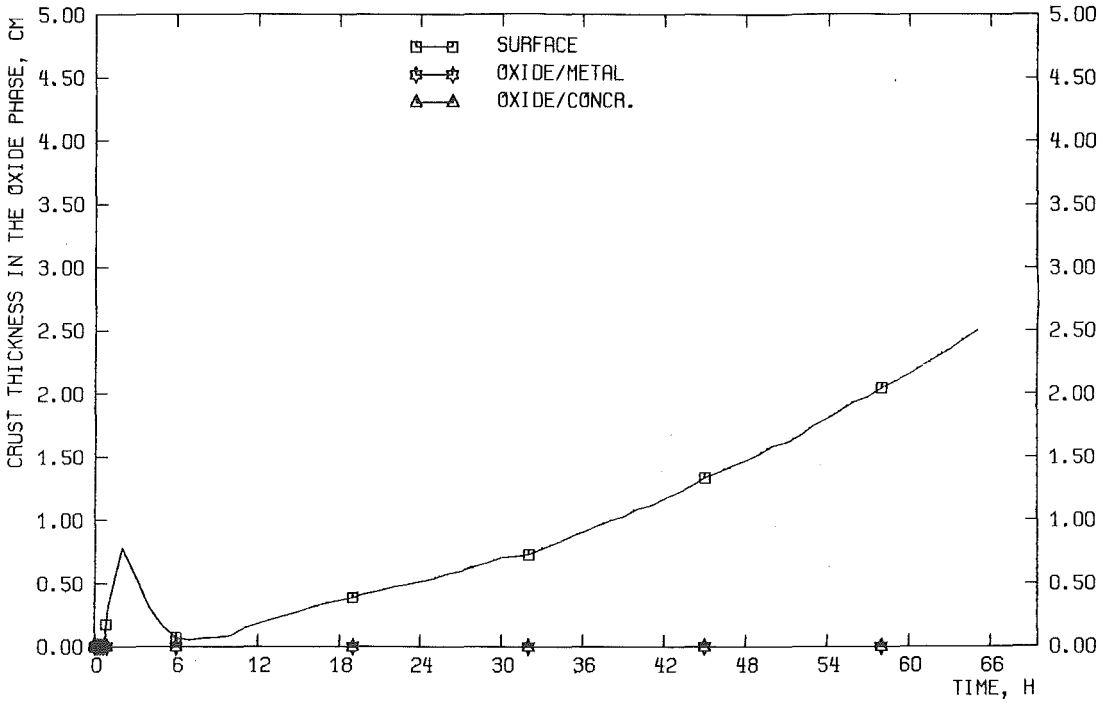


Fig. 44: BWR melt crusts (mixed calculation).

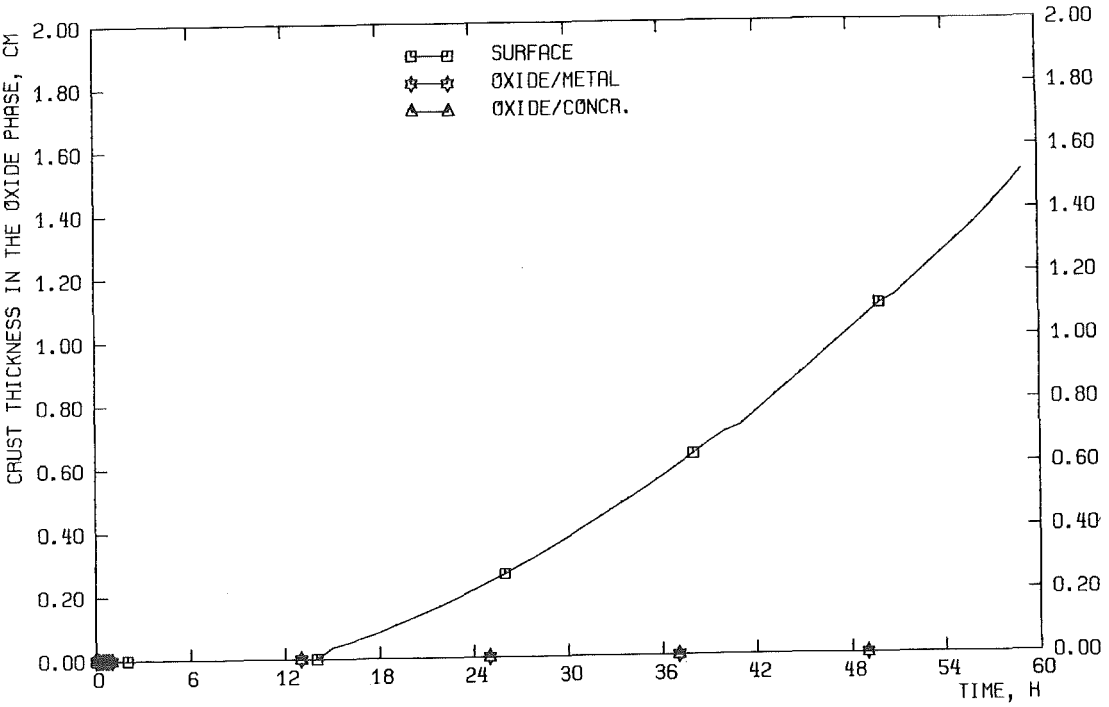


Fig. 45: BWR heat fluxes (mixed calculation).

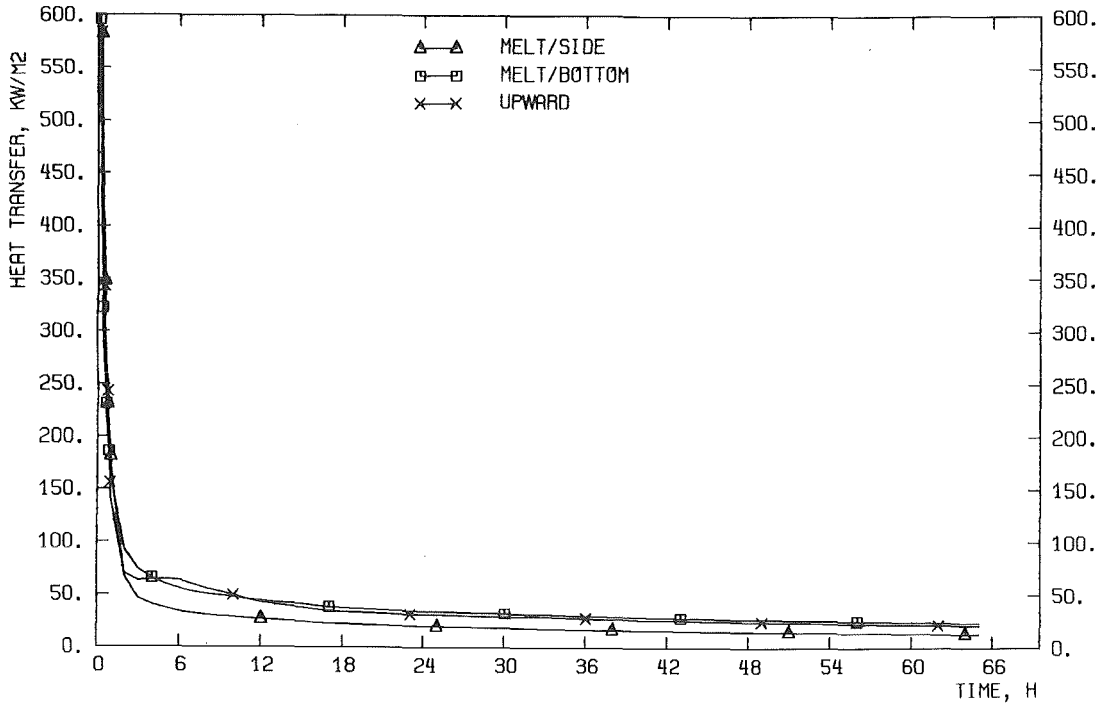


Fig. 46: BWR heat fluxes (mixed calculation).

4.4.2 Concrete Ablation

The calculated time of basemat penetration and the corresponding masses of eroded concrete are given in Table 10. The differences between the mixed and separated melt configurations are small.

| Melt Configuration | Mixed | Separated |
|---|---|---|
| Basemat penetration time (days) | 2.7 | 2.5 |
| Mass of eroded concrete (kg) | 1060 x $10^3$ | 982 x $10^3$ |

Table 10: WECHSL results for a BWR accident

The cavity profile for the mixed melt is shown in Figure 47 and that for the layered melt in Figure 48. The results presented are similar to those given in [3] for the mixed melt but differ significantly from those obtained for the stratified melt configuration obtained with the previous WECHSL version [18].

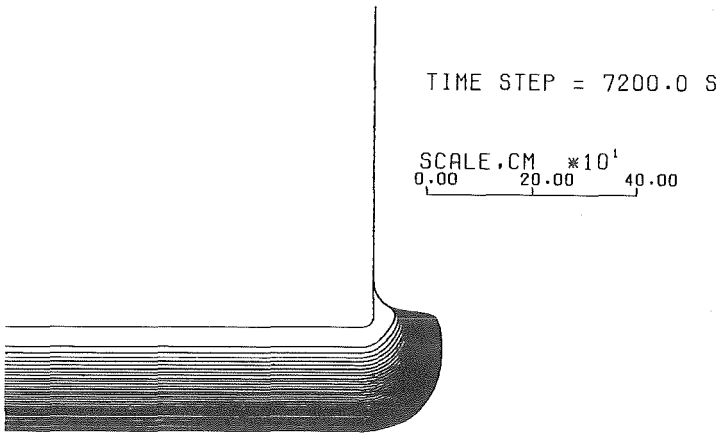


Fig. 47: BWR cavity erosion (mixed calculation).

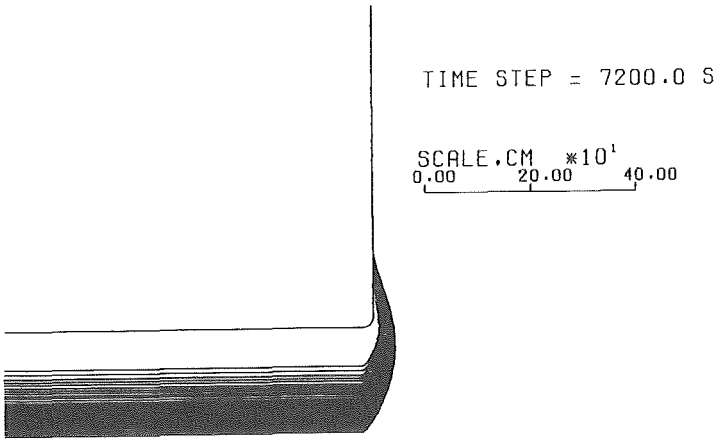


Fig. 47: BWR cavity erosion (mixed calculation).

### 4.2.3 Chemistry and Gas Release

The oxidation times of Zr and Si are listed in Table 11.

| Melt Configuration | Duration of the Oxidation Process [s] | |
|---|---|---|
| | Zr chemistry | Si chemistry |
| Mixed | 488 | $3.4798 \times 10^4$ |
| Layered | 68 | $2.0706 \times 10^4$ |

Table 11: Oxidation times in a BWR accident.

The corresponding gas release rates and total amount of gases predicted by WECHSL are represented in Figures 49-50 for the mixed melt and in Figures 51-52 for the layered melt calculations. In the early period of the concrete erosion process the gas release rates as well as the composition of the released gases differ significantly for the mixed and the layered melt configurations. The total amount of released gases is related to the mass of eroded concrete and, therefore, the predicted values are similar for both calculations in accordance with Table 11.

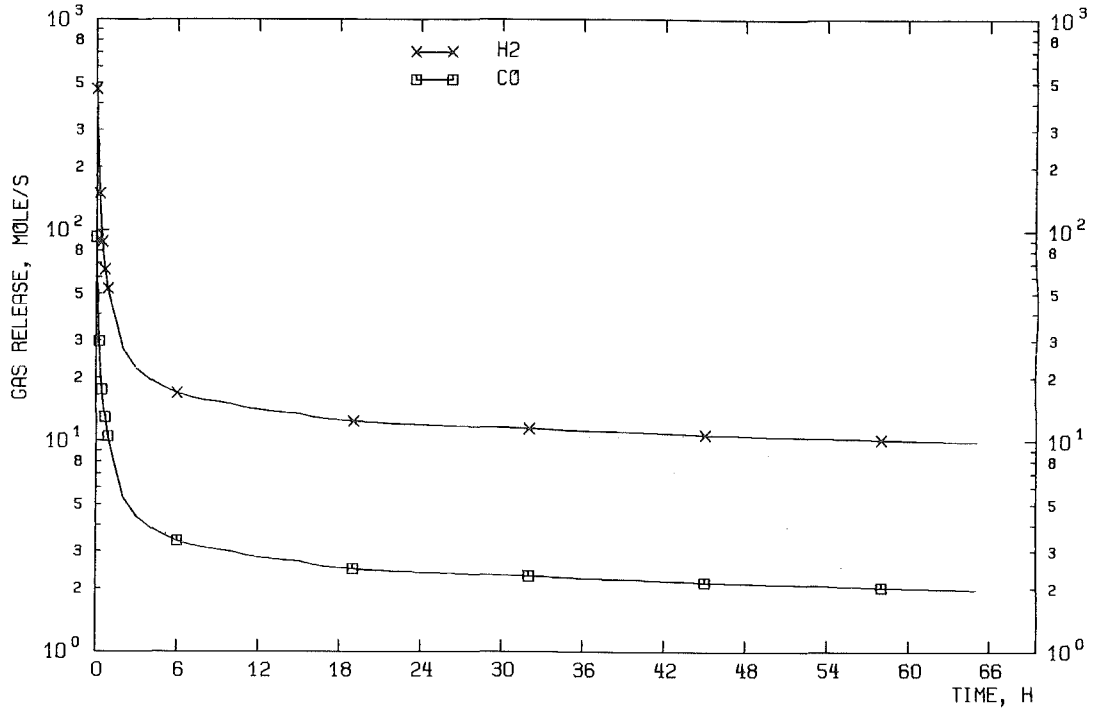


Fig. 49: BWR gas release rated (mixed calculation).

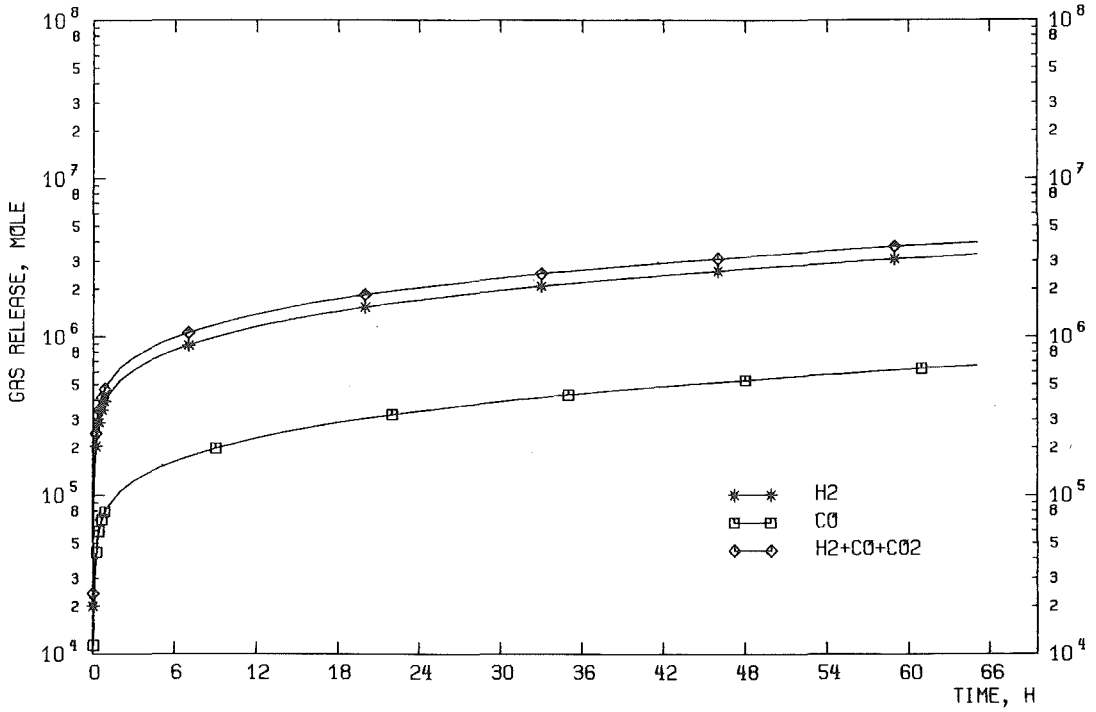


Fig. 50: BWR integrated gas release (mixed calculation).

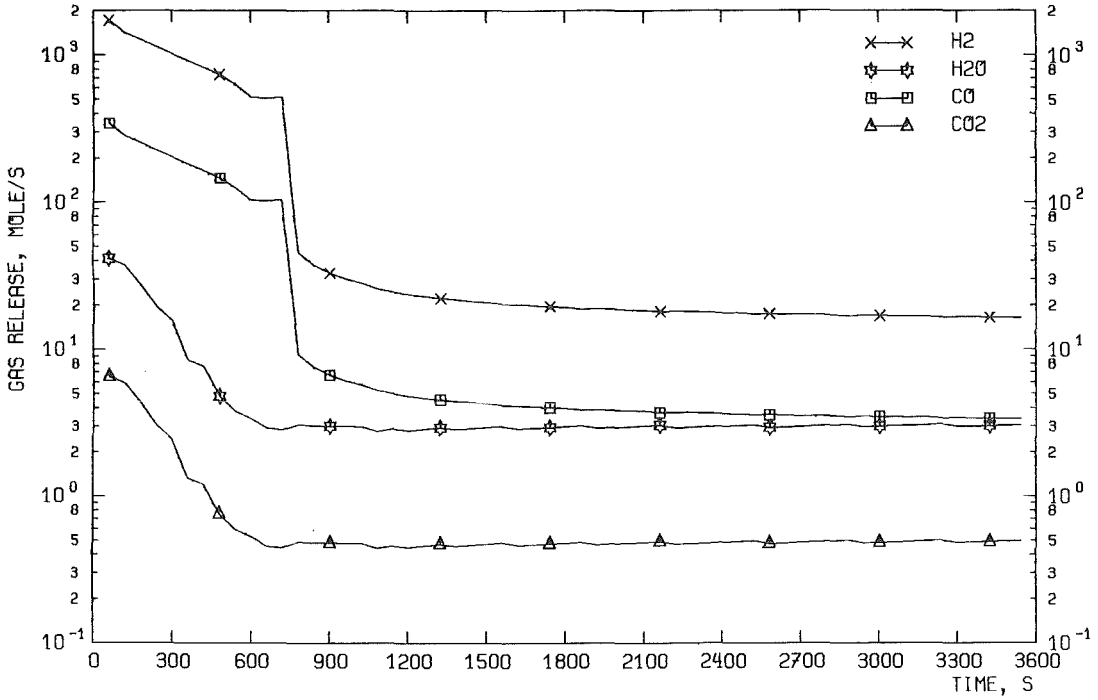


Fig. 51: BWR gas release rates (mixed calculation).

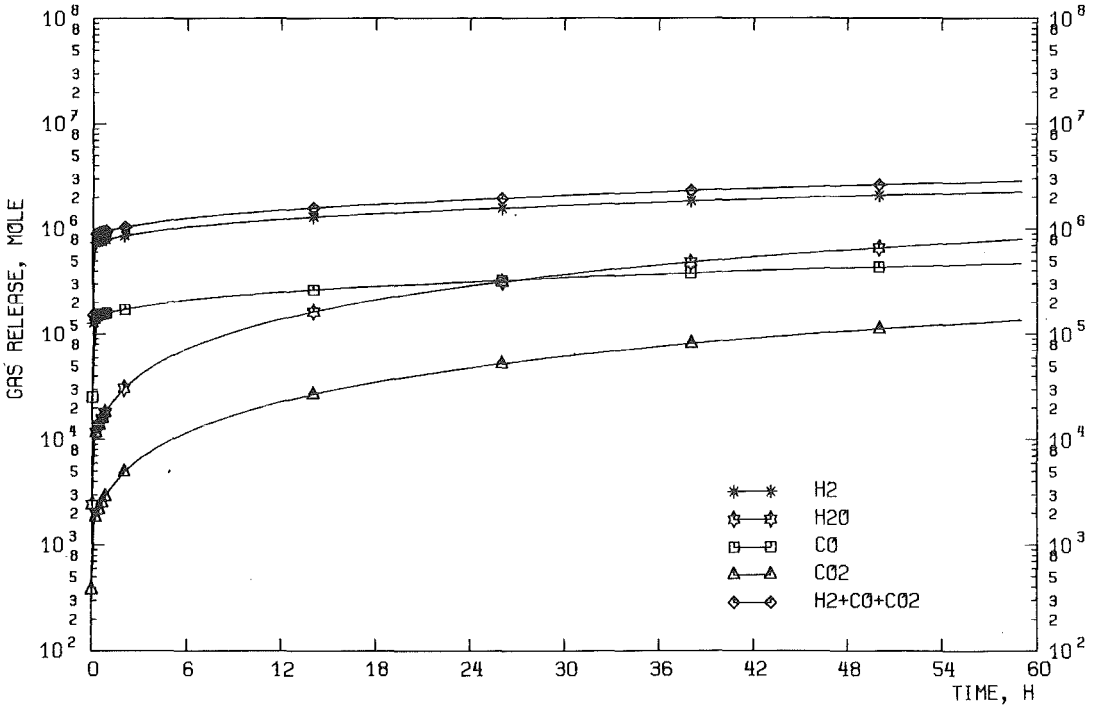


Fig. 52: BWR integrated gas release (layered calculation).

## 5. Conclusions

The current level of agreement with experimental data would appear to be good enough to justify the use of the WECHSL code in risk assessment studies, provided the uncertainties in the predicted results are taken into account. However, plant calculations still require extrapolation beyond the existing experimental database; in particular the treatment of long-term radial ablation by an oxide melt (which then affects the predictions for axial ablation) could not be validated sufficiently because of lack of experimental data. There is only one oxide test including two-dimensional concrete erosion.

The various accident scenarios result in a broad variation of the initial conditions of the melt at the time of RPV failure. There are also uncertainties in the knowledge of the properties of core melts, among others the viscosity, the solidus-liquidus temperatures, and the thermal conductivity of the ex-vessel oxide melts. The PWR core melt accident which had been the subject of the investigations in the German Risk Study Phase B was used as the reference case to assess the uncertainties in WECHSL MCCI calculations which are caused by the variations mentioned above.

In contrast to the cavity shapes predicted by the former WECHSL versions for a stratified melt configuration, the current WECHSL code predicts cavities without step in the axial ablation front which corresponded to the ablation of an annulus by the oxide phase around the frozen metal layer. Another important difference with respect to former results consists in the higher oxide melt temperatures predicted by the current WECHSL version. Variations of the initial melt temperature, the use of a high solidus temperature as well as a low solidus temperature of the oxide melt and the variation of the extent of Zr oxidation of the corium at the beginning of core-concrete interaction influenced only the short term MCCI predictions. Also, only a weak influence on WECHSL results was observed in calculations using different thermal conductivities in solid crusts. The strongest impact on WECHSL MCCI predictions was due to variations of the viscosity of the oxide melt. In calculations with an increased viscosity much higher melt temperatures were predicted. In addition, the partition to the concrete of the radial and axial heat fluxes was different from that in the standard calculation. This led to a cavity shape with a more pronounced axial erosion and, therefore, to a time of basemat erosion which is reduced to 3/4 of the reference value. In general, it can be stated that despite the existing uncertainties the use of the WECHSL code, in risk assessment studies can be justified.

## 6. References


[1] D. R. Bradley. D. R. Gardner, J. E. Brockmann, and R. O. Griffith: CORCON-Mod3: An Integrated Computer Model for Analysis of Molten Core-Concrete Interactions.
NUREG/CR-5843 [SAND92-0167], October 1993.

[2] J. J. Foit, M. Reinmann, B. Adroguer, G. Cenerino, S. Stiefel
The WECHSL-Mod3 Code: A Computer Program for the Interaction of a Core Melt with Concrete Including the Long Term Behavior Model Description and User's Manual
FZKA 5416 (1995).

[3] J. J. Foit, L. D. Howe: Plant Applications of CORCON/WECHSL in: Molten Corium/Concrete Interaction and Corium Coolability - A State of the Art Report -
Directorate - General XII Science, Research and Development (1995), 130-179.

[4] E. R. Copus: Sustained Uranium Dioxide/Concrete Interaction Tests.
Proceedings of the Second OECD (NEA) CSNI Specialist Meeting on Molten Core Debris-Concrete Interaction, Karlsruhe, April 1992
KfK 5108 (NEA/CSNI/R (92) 10), 51-66.

[5] D. H. Thompson, J. K. Fink, D. R. Armstrong, B. W. Spencer, B. R. Sehgal: Thermal-Hydraulic Aspects of the Large-Scale Integral MCCI Tests in the ACE Program
Proceedings of the Second OECD (NEA) CSNI Specialist Meeting on Molten Core Debris-Concrete Interaction, Karlsruhe, April 1992
KfK 5108 (NEA/CSNI/R (92) 10), 97-110.

[6] H. Alsmeyer:
BETA Experiments on Zirconium Oxidation and Aerosol Release during Melt-Concrete Interaction
Proceedings of the Second OECD (NEA) CSNI Specialist Meeting on Molten Core Debris-Concrete Interaction, Karlsruhe, April 1992
KfK 5108 (NEA/CSNI/R (92) 10), 67-82

[7] C. Renault, J. J. Foit, and J. Poublan:
WECHSL-Mod3 Assessment Report
Note Technique Semar 92/93 KfK 5164 (1992).

[8] J. J. Foit: Developments of the WECHSL Code Related to the Analysis of Recent BETA V5.1 Experiments, ANP '92. Intern. Conf. on Design and Safety of Adv. Nuclear Power Plants, Oct. 25 - 29, 1992, Tokyo, Japan, Proc. Vol. III, P12.3-1.

[9] J. J. Foit, A. Miassoedov: Modeling of Viscosity and Heat Transfer of Complex Oxidic Melts in WECHSL, FZKA 5507 (1995).

[10] F. Parozzi, M. Vidard, D. Fioravanti, S. Locatelli:
Main Objectives of MCCI for NPP Safety Analysis in: Molten Corium/Concrete Interaction and Corium Coolability - A State of the Art - Directoriate - General XII Science, Research and Development (1995), 1-28.

[11] Deutsche Risikostudie Kernkraftwerke, Phase B -: eine Untersuchung / Ges. für Reaktorsicherheit. Im Auftr. D. Bundesministers für Forschung u. Technologie. - Köln: Verl. TÜV Rheinland, 1990.

[12] A. Skokan, H. Hollek, M. Peehs:
"Chemical Reactions between Light Water Reactor Core Melt and Concrete", Nucl. Techn. 46 (1979)2, 255-262.

[13] C. Renault, J. J. Foit: Assessment Status of the WECHSL-MOD3 Code,
Proceedings of the Second OECD (NEA) CSNI Specialist Meeting on Molten Core Debris-Concrete Interaction, Karlsruhe, April 1992
KfK 5108 (NEA/CSNI/R (92) 10), 157-171.

[14] G. Gliemeroth, G. Müller:
Glas und Glaskeramik
Ullmanns Enzyklopädie der technischen Chemie
4. Aufl. Band 12, Verlag Chemie, Weinheim-New York (1976).

[15] M. F. Roche, D. V. Steidl, L. Leibowitz, J. K. Fink, b. Raj Sehgal:
"Vicosity of Corium Concrete Mixtures at High Temperatures."
ACE-TR-C37 (1994).

[16] A. Miassoedov, J. J. Foit:
Unveröffentlicher Bericht, Kernforschungszentrum Karlsruhe (1993).

[17] A. Commandé: Corium-Concrete Interaction Study of Heat Conduction in the Concrete, Comparisons with WECHSL, Note Technique SEMAR 94/55.

[18] J. J. Foit: Assessment of Reactor Accident Scenarios Using WECHSL Code, Proceedings of the Third Workshop on Severe Accident Research in Japan November 4-6, 1992, Tokyo, Japan, March 1993, (Ed.) Jun Sugimoto, 440-445.